Commun. Comput. Phys.
doi: 10.4208/cicp.OA-2025-0108

Vol. **39**, No. 3, pp. 661-695
March 2026

Structure-Preserving SAV-RKs Spectral Methods for Nonlinear Hamiltonian System

Jie Shen[1], Lianpeng Xue[2,3] and Qifeng Zhang[2,*]

[1] *School of Mathematical Science, Eastern Institute of Technology, Ningbo, 315200, P.R. China.*
[2] *Department of Mathematics, Zhejiang Sci-Tech University, Hangzhou, 310018, P.R. China.*
[3] *Department of Mathematics, Shanghai Normal University, Shanghai, 200234, P.R. China.*

Received 24 April 2025; Accepted (in revised version) 29 August 2025

Abstract. It is well-established that high-order symplectic Runge–Kutta methods cannot preserve polynomial energy of Hamiltonian systems beyond degree two. However, the scalar auxiliary variable (SAV) approach, which was originally proposed for gradient flow systems, offers an effective strategy to overcome this limitation, albeit with a modified energy. In this paper, we study high-order Runge–Kutta methods for solving general Hamiltonian systems without imposing a lower bound on the high-order part of the energy functional. By integrating a symplectic Runge–Kutta method with a new SAV strategy, we develop a class of high-order nonlinear structure-preserving s-stage Runge–Kutta SAV (SAV-RKs) spectral methods, and prove that the nonlinear semi-discrete scheme can preserve the Hamiltonian energy and other conservative quantities such as mass/momentum (if they exist). In addition, we design a tailored fast Newton iteration algorithm to efficiently solve the resulting nonlinear algebraic system. Finally, we carry out extensive numerical simulations on several benchmark problems, including cases where the energy functional is either bounded or unbounded, to validate the accuracy and robustness of the proposed algorithms.

AMS subject classifications: 65M06, 65M12
Key words: Hamiltonian system, symplectic Runge–Kutta method, SAV approach, spectral method.

1 Introduction

Hamiltonian systems play a pivotal role in the study of classical mechanics and have found extensive applications in various fields, including quantum mechanics and statis-

*Corresponding author. *Email addresses:* jshen@eitech.edu.cn (J. Shen), lpxue@mails.zstu.edu.cn (L. Xue), zhangqifeng0504@gmail.com (Q. Zhang)

tical mechanics. A Hamiltonian system is characterized by a scalar function known as the Hamiltonian, which typically represents the total energy of the system and remains unchanging over time.

In this paper we are concerned with a class of Hamiltonian systems in the form of

$$\partial_t u = \mathcal{D}\frac{\delta H}{\delta u}, \quad t \in (0,T], \tag{1.1}$$

where $\mathcal{D}$ is a skew-adjoint operator, u is a function defined on $\mathbb{V}$ ($\mathbb{V}=\mathbb{C}$ or $\mathbb{R}$), and $\frac{\delta H}{\delta u}$ represents the variational derivative of H with respect to u. The Hamiltonian energy $H:=H[u]$ satisfies

$$H := H_L + H_N,$$

where

$$\frac{\delta H_L}{\delta u} = \mathcal{L}u, \quad \frac{\delta H_N}{\delta u} = \mathcal{N}u$$

with $\mathcal{L}$ and $\mathcal{N}$ representing linear and nonlinear operators, respectively.

The system (1.1) encompasses many important equations in classical mechanics, quantum physics and nonlinear optics. Notable examples include the Camassa–Holm (CH) equation [3], the Korteweg–de Vries (KdV) equation [32], the nonlinear Schrödinger (NLS) equation [10], the derivative nonlinear Schrödinger (DNLS) equation [4,24], which play significant roles in the field of the nonlinear optics [30,33,34,41], among others.

Due to the antisymmetry of the operator $\mathcal{D}$, it is straightforward to deduce that the system (1.1) conserves the Hamiltonian energy, i.e.,

$$\frac{\mathrm{d}}{\mathrm{d}t}H = \Big(\frac{\delta H}{\delta u}, \partial_t u\Big) = \Big(\frac{\delta H}{\delta u}, \mathcal{D}\frac{\delta H}{\delta u}\Big) = 0. \tag{1.2}$$

The invariant

$$\frac{\mathrm{d}}{\mathrm{d}t}(u,1) = 0 \tag{1.3}$$

is also conserved provided that $\mathcal{D}$ is a linear differential operator. In addition, Hamiltonian systems may conserve other quantities such as mass/momentum, etc. We shall assume that the solution of the system (1.1) also satisfies

$$\frac{\mathrm{d}}{\mathrm{d}t}(u,\mathcal{B}u) = 0, \tag{1.4}$$

where $\mathcal{B}$ is a linear symmetric (algebraic or differential) operator. Some specific examples will be provided in the next section. Preserving these invariant properties in a numerical scheme is highly desirable, as it ensures that the discrete solution preserves the essential features of the original differential equation.

Over the past few decades, significant efforts have been devoted to developing efficient and accurate numerical methods capable of preserving as many conservation laws

of Hamiltonian systems as possible. On the side of spatial discretization, notable contributions include: the finite difference method [7], finite element method [23], spectral method [19,36], discontinuous Galerkin method [5] (cf. also the references therein). On the other hand, prominent approaches for the temporal discretization include: symplectic geometric algorithms [8,9], Runge–Kutta methods [29,31,51], integrating factor methods [18,27], exponential time differencing methods [12], and so on. Other techniques include parametric symplectic partitioned methods [43], operator splitting method [17], invariant energy quadratization (IEQ) method [50], deep learning method [20,35,44] (cf. also the references therein).

In recent years, the SAV approach [37,38] and its related variants have gained popularity in developing structure-preserving schemes for gradient type flows and Hamiltonian systems. These include applications to Allen-Cahn equation and Cahn-Hillard equation [1,39], the fractional nonlinear Schrödinger equation [11], the nonlinear Klein-Gordon equation [21], the Gross–Pitaevskii equation [6] and many others. A key technical assumption of the SAV approach is that the high-order nonlinear part of the energy functional has a lower bound [38]. Unfortunately, many problems do not automatically meet this assumption, such as the Korteweg–de Vries equation [47] and the second-type derivative nonlinear Schrödinger (DNLSII) equation [4]. On the other hand, Lubich et al. [15] (see Theorem 3.3) pointed out an unfortunate fact that no Runge–Kutta method can preserve all polynomial invariants of degree n $(n\geqslant 3)$. This negative result prompts the study of new numerical methods capable of preserving high-order invariants.

Recently, Yang combined the high-order implicit Runge–Kutta methods with the SAV approach to the generalized KdV equation [48] and generalized Benjamin-Ono equation [47], both of which are special cases of Hamiltonian systems. This work successfully constructed numerical schemes capable of preserving higher-order (reformulated) Hamiltonian energy under the assumption that the high-order part of the energy functional is lower bounded. However, many Hamiltonian systems, such as the KdV equation, do not satisfy this *priori* assumption. *A natural question is whether a proper combination of the high-order implicit Runge–Kutta method and the SAV approach can preserve higher-order (reformulated) Hamiltonian energy for more general Hamiltonian systems without assuming a lower bound for the high-order part of the energy functional*?

The main purpose of this paper is to give a positive answer to the above question. Our main contributions are summarized below:

- We propose a class of nonlinear high-order SAV-RK*s* methods which can preserve reformulated Hamiltonian energy, (1.3) and (1.4), for general Hamilton systems without assuming a lower bound for the high-order nonlinear part of the energy.
- We develop a fast linearized Newton iteration algorithm for solving the nonlinear system resulting from the SAV-RK*s* methods.
- We carry out ample numerical simulations on a series of benchmark problems with Hamiltonian structures to confirm the effectiveness and robustness of the proposed schemes.

We note that the usual SAV approach leads to linear schemes but fails to preserve the original second-order conservation laws (Corollary 3.1 after Theorem 3.1), while the SAV-RK*s* schemes proposed in this paper are nonlinear but capable of preserving the original higher-order energy, and the cost of solving nonlinear systems can be significantly reduced by a fast linearized Newton iteration algorithm.

The remainder of this paper is organized as follows. In Section 2, we first list some typical Hamilton systems and derive an equivalent system with a reformulated Hamiltonian energy. In Section 3, we construct the temporal semi-discretization by using the symplectic Runge–Kutta method for the equivalent system, followed by the construction of spatial discretization with Fourier pseudo-spectral method and full discretization in Section 4. In Section 5, we develop a fast solver for the nonlinear system at each time step of the discretization. In Section 6, several numerical examples of classical Hamiltonian systems are provided to verify the effectiveness of our selection strategy. Concluding remarks are provided in Section 7.

2 Some typical examples and the SAV approach

We first present in this section some specific Hamiltonian systems that we shall consider in this paper, followed by a reformulation of (1.1) based on the SAV approach.

2.1 Some specific Hamiltonian systems

For the sake of simplicity, we consider $\Omega \subset \mathbb{R}$ with periodic boundary conditions. Similarly, one can consider extensions to Hamiltonian systems in multi-dimension with other suitable boundary conditions by using spectral methods with Chebyshev polynomials [40] or penalty techniques [16].

- The Korteweg–de Vries (KdV) equation (see, e.g., [26]):

$$\partial_t u = -\partial_x \Big(\partial_x^2 u + \frac{1}{2} u^2 \Big). \tag{2.1}$$

  The corresponding Hamiltonian energy is

$$H[u] := \frac{1}{2}(\partial_x u, \partial_x u) - \frac{1}{6}(u^3, 1).$$

  Hence, $H_N = -\frac{1}{6}(u^3,1)$ may not have a lower bound. The problem (2.1) has two additional conservation laws, expressed as

$$M_1[u] := (u,1); \quad M_2[u] := (u, \mathcal{B}u) \quad \text{with} \quad \mathcal{B} = \mathcal{I},$$

  where $\mathcal{I}$ denotes the identity operator. It is clear that $\mathcal{D} = \partial_x$ for this problem.

- The nonlinear Schrödinger (NLS) equation:

$$\mathrm{i}\partial_t u+\partial_x^2 u+2|u|^2 u=0. \tag{2.2}$$

The first three conservative quantities read

$$\begin{aligned}&M_2[u]:=(u,\mathcal{B}u)\equiv M_2[u_0],\quad \text{with}\quad \mathcal{B}=\mathcal{I}\text{ or }-\mathrm{i}\partial_x,\\&H[u]:=(\partial_x u,\partial_x u)-(u^2,u^2)\equiv H[u_0].\end{aligned}$$

With the help of $H[u]$ above, the problem (2.2) can be converted into a Hamiltonian system

$$\begin{pmatrix}u\\ \bar{u}\end{pmatrix}=\mathcal{D}\begin{pmatrix}\frac{\delta H}{\delta u}\\ \frac{\delta H}{\delta \bar{u}}\end{pmatrix},\quad \mathcal{D}=\begin{pmatrix}0 & -\mathrm{i}\\ \mathrm{i} & 0\end{pmatrix}.$$

- The first-type derivative nonlinear Schrödinger (DNLSI) equation (see, e.g., [2,24]):

$$\mathrm{i}\partial_t u+\partial_x^2 u+\mathrm{i}\partial_x(|u|^2 u)=0. \tag{2.3}$$

The problem (2.3) has the following conserved quantities

$$\begin{aligned}&M_1[u]:=(u,1)\equiv M_1[u_0],\\&M_2[u]:=(u,\mathcal{B}u)\equiv M_2[u_0],\quad \text{with}\quad \mathcal{B}=\mathcal{I},\\&H[u]:=\mathrm{i}(u,\partial_x u)+\frac{1}{2}(u^2,u^2)\equiv H[u_0].\end{aligned}$$

In a similar manner, the problem (2.3) can be transformed into a Hamiltonian system

$$\begin{pmatrix}u\\ \bar{u}\end{pmatrix}=\mathcal{D}\begin{pmatrix}\frac{\delta H}{\delta u}\\ \frac{\delta H}{\delta \bar{u}}\end{pmatrix},\quad \mathcal{D}=\begin{pmatrix}0 & -\partial_x\\ -\partial_x & 0\end{pmatrix}.$$

- The second-type derivative nonlinear Schrödinger (DNLSII) equation (see, e.g., [4]):

$$\mathrm{i}\partial_t u+\partial_x^2 u+\mathrm{i}|u|^2\partial_x u=0. \tag{2.4}$$

It is straightforward to show that the DNLSII equation (2.4) conserves the Hamiltonian

$$H[u]:=(\partial_x u,\partial_x u)+\frac{\mathrm{i}}{4}(\partial_x u^2,u^2)\equiv H[u_0].$$

It also has two additional conservation laws

$$M_2[u]:=(u,\mathcal{B}u)\equiv M_2[u_0],\quad \text{with}\quad \mathcal{B}=\mathcal{I}\text{ or }-\mathrm{i}\partial_x.$$

Clearly, the boundedness of the high-order energy functional $\frac{\mathrm{i}}{4}(\partial_x u^2,u^2)$ cannot be guaranteed. Using variational derivatives and matrix calculation, we can also convert it into the following Hamiltonian form:

$$\begin{pmatrix}u\\ \bar{u}\end{pmatrix}=\mathcal{D}\begin{pmatrix}\frac{\delta H}{\delta u}\\ \frac{\delta H}{\delta \bar{u}}\end{pmatrix},\quad \mathcal{D}=\begin{pmatrix}0 & -\mathrm{i}\\ \mathrm{i} & 0\end{pmatrix}.$$

- The Camassa–Holm (CH) equation (see, e.g., [3,22]):

$$\partial_t u-\partial_t\partial_x^2 u+3u\partial_x u-2\partial_x u\partial_x^2 u-u\partial_x^3 u=0. \tag{2.5}$$

The problem (2.5) has the following conserved quantities

$$\begin{aligned}&M_1[u]:=(u,1)\equiv M_1[u_0],\\&M_2[u]:=(u,\mathcal{B}u)\equiv M_2[u_0],\quad \text{with}\quad \mathcal{B}=\mathcal{I}-\partial_x^2,\\&H[u]:=-\frac{1}{2}(u,u^2+(\partial_x u)^2)\equiv H[u_0].\end{aligned}$$

Using the variational derivative of $H[u]$, the problem (2.5) can be reformulated as a Hamiltonian system

$$\partial_t u=\mathcal{D}\frac{\delta H}{\delta u}=\mathcal{D}\Big(-\frac{3}{2}u^2-\frac{1}{2}(\partial_x)^2+\partial_x(u\partial_x u)\Big),$$

with $\mathcal{D}=(\mathcal{I}-\partial_x^2)^{-1}\partial_x$.

2.2 Reformulation based on the SAV approach

In this section, we introduce a scalar auxiliary variable v to reformulate the system (1.1) into an equivalent one. The original SAV approach assumes that the high-order nonlinear part of the energy, H_N, has a lower bound. However, this assumption does not hold for some certain important Hamiltonian systems. To address this limitation, we propose a modified SAV approach to remove this assumption. Without loss of generality, we define a quadratic functional $M[u]$ with a lower bound, for example, $M[u]:=(u,u)+\delta$ where $\delta>0$ is arbitrary. Then we have

$$H[u]=H[u]-M[u]+M[u]=H[u_0].$$

Therefore, we can define a scalar auxiliary variable as

$$v(t):=\sqrt{H[u_0]-H[u]+M[u]}=\sqrt{M[u]}>0. \tag{2.6}$$

And differentiating v, we have

$$\frac{\mathrm{d}}{\mathrm{d}t}v=\frac{\frac{\mathrm{d}}{\mathrm{d}t}(H[u_0]-H[u]+M[u])}{2\sqrt{H[u_0]-H[u]+M[u]}}=-\frac{1}{2}\Big(\frac{\frac{\delta}{\delta u}(H[u]-M[u])}{\sqrt{M[u]}},\partial_t u\Big).$$

Then, we expand the system (1.1) to

$$\begin{cases}\partial_t u=\mathcal{D}\Big[\dfrac{\frac{\delta}{\delta u}(H[u]-M[u])}{\sqrt{M[u]}}\cdot v+\dfrac{\delta M}{\delta u}\Big],\\[2ex]\dfrac{\mathrm{d}}{\mathrm{d}t}v=-\dfrac{1}{2}\Big(\dfrac{\frac{\delta}{\delta u}(H[u]-M[u])}{\sqrt{M[u]}},\partial_t u\Big).\end{cases} \tag{2.7}$$

The initial value conditions corresponding to the system (2.7) become

$$u(x,0)=u_0(x),\quad v(0)=\sqrt{M[u_0]}.$$

The original energy corresponding to the system (2.7) can be expressed as

$$E[u,v]:=-v^2+M[u]+H[u_0],\quad t\in[0,T]. \tag{2.8}$$

We obtain immediately from the first equation in (2.7) that (1.3) still holds. On the other hand, assuming (1.4) holds in the original Hamiltonian flow, it still holds for the reformulated system (2.7) since the first equation in (2.7) deduces to (1.1) because of $v(t)=\sqrt{M[u]}$.

Remark 2.1. The choice of the quadratic functional $M[u]$ is not unique. Alternatives such as $(\partial_x u,\partial_x u)$ and $(\partial_x^2 u,\partial_x^2 u)$ can also be utilized, which, overall, do not affect the long time simulations numerically. We choose $M[u]=(u,u)+\delta$ with $\delta>0$ since it does not require extra regularization of the solution.

Remark 2.2. The equivalent reformulation (2.7) is also available for the gradient flow system, see, e.g., [37, 38]. In this case, it is only necessary to replace the entire $\sqrt{M[u]}$ in (2.7) with $\sqrt{H[u_0]-H[u]+M[u]}$.

3 Semi-discrete (in time) schemes

In this section, we describe the temporal discretization of the equivalent system (2.7) based on the symplectic Runge–Kutta method.

Denote coefficients $\mathbf{A}=(a_{ij})_{s\times s}$, $\mathbf{b}=(b_1,b_2,\cdots,b_s)^T$ and $\mathbf{c}=(c_1,c_2,\cdots,c_s)^T$. The Runge–Kutta method is given by the Butcher tableau

$$\begin{array}{c|c} \mathbf{c} & \mathbf{A} \\ \hline & \mathbf{b}^T \end{array}.$$

We list the Butcher Tableau of the s-stage Gaussian-Legendre Runge–Kutta (RKs) method for $s=1,2,3,4$ in Appendix A.

Denote the numerical solutions in the temporal semi-discrete setting by $u^k\approx u(x,t_k)$ and $v^k\approx v(t_k)$, and let the intermediate values $U_i=u(x,t_k+c_i\tau)$ and $V_i=v(t_k+c_i\tau)$ present the exact solutions satisfying (2.7) at the time $t=t_k+c_i\tau$.

For simplicity, we rewrite (2.7) as

$$\begin{cases} \partial_t u=f(u,v), \\ \dfrac{\mathrm{d}}{\mathrm{d}t}v=g(u,v). \end{cases} \tag{3.1}$$

Then, the application of RK*s* to (3.1) leads to

$$\begin{cases} u^{k+1}=u^k+\tau\sum\limits_{i=1}^{s}b_i f_i, \quad U_i=u^k+\tau\sum\limits_{j=1}^{s}a_{ij}f_j, \\ v^{k+1}=v^k+\tau\sum\limits_{i=1}^{s}b_i g_i, \quad V_i=v^k+\tau\sum\limits_{j=1}^{s}a_{ij}g_j, \end{cases} \tag{3.2}$$

where $f_i=f(U_i,V_i)$ and $g_i=g(U_i,V_i)$.

We first show that the symplectic Runge–Kutta method preserves the reformulated energy and other conserved quantities (if they exist) no higher than degree two.

Theorem 3.1. *Denote* $E^k=E[u^k,v^k]$, $M_i^k=M_i[u^k]$ $(i=1,2)$ *and* $H^0=H[u_0]$. *Then, the s-stage symplectic Runge–Kutta method* (3.2) *satisfying*

$$b_ia_{ij}+b_ja_{ij}-b_ib_j=0 \quad \textit{for} \quad i,j=1,2,\cdots,s, \tag{3.3}$$

preserves mass (1.3), (1.4) *and the Hamiltonian energy* (2.8), *i.e.,*

$$M_1^{k+1}=M_1^k, \quad M_2^{k+1}=M_2^k, \quad E^{k+1}=E^k.$$

Proof. According to the first equation in (3.1) and exact conservation of M_1 in (1.3), we have

$$(f_i,1)=(\partial_t U_i,1)=\frac{\mathrm{d}}{\mathrm{d}t}(U_i,1)=\frac{\mathrm{d}}{\mathrm{d}t}M_1[U_i]=0.$$

Therefore,

$$M_1^{k+1}=(u^{k+1},1)=(u^k+\tau\sum_{i=1}^{s}b_i f_i,1)=(u^k,1)+\tau\sum_{i=1}^{s}b_i(f_i,1)=M_1^k.$$

Next, utilizing first equation in (3.1) again and conservation of M_2 in (1.4), we have

$$(U_i,\mathcal{B}f_i)+(f_i,\mathcal{B}U_i)=(U_i,\mathcal{B}\partial_t U_i)+(\partial_t U_i,\mathcal{B}U_i)=\frac{\mathrm{d}}{\mathrm{d}t}(U_i,\mathcal{B}U_i)=\frac{\mathrm{d}}{\mathrm{d}t}M_2[U_i]=0.$$

Therefore,

$$\begin{aligned} M_2^{k+1}&=(u^{k+1},\mathcal{B}u^{k+1})=(u^k+\tau\sum_{i=1}^{s}b_i f_i,\mathcal{B}u^k+\tau\sum_{i=1}^{s}b_i\mathcal{B}f_i) \\ &=(u^k,\mathcal{B}u^k)+\tau\sum_{i}^{s}b_i[(u^k,\mathcal{B}f_i)+(f_i,\mathcal{B}u^k)]+\tau^2\sum_{i,j=1}^{s}b_ib_j(f_i,\mathcal{B}f_j) \\ &=(u^k,\mathcal{B}u^k)+\tau\sum_{i}^{s}b_i[(U_i,\mathcal{B}f_i)+(f_i,\mathcal{B}U_i)] \\ &\quad+\tau^2\sum_{i,j=1}^{s}(b_ib_j-b_ia_{ij}-b_ja_{ij})(f_i,\mathcal{B}f_j)=M_2^k. \end{aligned}$$

Finally, we prove $E^{k+1}=E^k$. Without loss of generality, we assume $M[u]=(u,u)$. First, differentiating the conservation law (2.8) with respect to t, we have

$$0=\frac{\mathrm{d}}{\mathrm{d}t}(U_i,U_i)-\frac{\mathrm{d}}{\mathrm{d}t}(V_i)^2=(U_i,f_i)+(f_i,U_i)-2g_iV_i,\quad i=1,2,\cdots,s. \tag{3.4}$$

Then, by the definition of the semi-discrete energy, we have

$$\begin{aligned}
E^{k+1}&=(u^{k+1},u^{k+1})-(v^{k+1})^2+H^0\\
&=((u^k+\tau\sum_{i=1}^s b_if_i),(u^k+\tau\sum_{i=1}^s b_if_i))-(v^k+\tau\sum_{i=1}^s b_ig_i)^2+H^0\\
&=(u^k,u^k)-(v^k)^2+H^0+\tau^2\sum_{i,j=1}^s b_ib_j\big[(f_i,f_j)-g_ig_j\big]\\
&\quad+\tau\big[(u^k,\sum_{i=1}^s f_i)+(\sum_{i=1}^s f_i,u^k)-2\sum_{i=1}^s b_ig_i\cdot v^k\big]\\
&=(u^k,u^k)-(v^k)^2+H^0+\tau^2\sum_{i,j=1}^s b_ib_j\big[(f_i,f_j)-g_ig_j\big]\\
&\quad+\tau\big[((U_i-\tau\sum_{j=1}^s a_{ij}f_j),\sum_{i=1}^s f_i)+(\sum_{i=1}^s f_i,U_i-\tau\sum_{j=1}^s a_{ij}f_j)\\
&\quad-2\sum_{i=1}^s b_ig_i\cdot(V_i-\tau\sum_{j=1}^s a_{ij}g_j)\big]\\
&=(u^k,u^k)-(v^k)^2+H^0+\tau\sum_{i=1}^s b_i\big[(U_i,f_i)+(f_i,U_i)-2g_iV_i\big]\\
&\quad+\tau^2\sum_{i,j=1}^s(b_ib_j-b_ia_{ij}-b_ja_{ij})\big[(f_i,f_j)-g_ig_j\big]=E^k,
\end{aligned}$$

where (3.3) and (3.4) have been utilized in the last equation.

This completes the proof. □

Similar to derivation of the semi-discrete scheme in [1], we can construct the following implicit-explicit scheme of the form

$$\begin{cases}
u^{k+1}=u^k+\tau\sum_{i=1}^s b_i\hat{f}_i, & U_i=u^k+\tau\sum_{j=1}^s a_{ij}\hat{f}_j,\\
v^{k+1}=v^k+\tau\sum_{i=1}^s b_i\hat{g}_i, & V_i=v^k+\tau\sum_{j=1}^s a_{ij}\hat{g}_j,
\end{cases} \tag{3.5}$$

where

$$\begin{cases} \hat{f}_i := \mathcal{D}\Big[\frac{\frac{\delta}{\delta u}(H[u]-M[u])}{\sqrt{M[u]}}\big|_{u=\hat{U}_i}\cdot V_i + \frac{\delta M}{\delta u}\big|_{u=U_i}\Big], \\ \hat{g}_i := -\frac{1}{2}\Big(\frac{\frac{\delta}{\delta u}(H[u]-M[u])}{\sqrt{M[u]}}\big|_{u=\hat{U}_i}, \hat{f}_i\Big) \end{cases}$$

with $\hat{U}_i$ some approximation to U_i.

Corollary 3.1. *The implicit-explicit numerical scheme* (3.5) *preserves the semi-discrete energy E^k, but it does not preserve the quadratic conservation M_2^k.*

Proof. Following a similar approach to the proof in Theorem 3.1, it can be shown that the numerical scheme (3.5) also preserves the semi-discrete energy E^k. However, it is obvious that scheme (3.5) does not preserve quadratic conservation law M_2^k due to $(U_i,\mathcal{B}\hat{f}_i)+(\hat{f}_i,\mathcal{B}U_i)\neq 0$. □

Remark 3.1. If the approximation order of $\hat{U}_i$ is lower than $2s$, the convergence rate of scheme (3.5) may fail to achieve the order $2s$ (see, e.g., [1]). Therefore, how to give a suitable approximation for the stage value $\hat{U}_i$ in the implicit-explicit scheme (3.5) poses a significant challenge.

4 Fully-discrete schemes

In this section, we first describe our spatial discretization based on the Fourier pseudo-spectral method. Then, we combine it with the semi-discrete (in time) schemes to derive fully-discrete schemes for the system (2.7) under an L-periodic boundary condition.

4.1 Spatial discretization

For simplicity, we assume that the problem is L-periodic and use the Fourier pseudo-spectral method. Let the periodic function $u(x,t)$ be approximated by $I_m u(x,t)$, which interpolates $u(x,t)$ at the following set of collocation points $x_j=jh$, $h=\frac{L}{m}$, $j=0,1,\cdots,m-1$, where m is an even number. The approximation $I_m u(x,t)$ takes the form

$$I_m u(x,t) = \sum_{j=0}^{m-1} u_j g_j(x), \tag{4.1}$$

where $u_j=u(x_j,t)$ and $g_j(x)$ is a trigonometric polynomial of degree $m/2$ given by

$$g_j(x) = \frac{1}{m}\sum_{l=-m/2}^{m/2}\frac{1}{c_l}\mathrm{e}^{\mathrm{i}\mu(x-x_j)l},$$

with

$$c_l=\begin{cases}1, & |l|<\frac{m}{2},\\ 2, & |l|=\frac{m}{2},\end{cases}\qquad \mu=\frac{2\pi}{L}.$$

One easily observes that $\{g_j\}_{j=0}^{m-1}$ satisfies the interpolation property $g_j(x_k)=\delta_j^k$. Differentiating (4.1) and evaluating the resulting expressions at the points $x_j, j=0,1,\cdots,m-1$, one has

$$\frac{\partial^k}{\partial_x^k}I_m u(x_j,t)=\sum_{l=0}^{m-1}u_l\frac{\mathrm{d}^k}{\mathrm{d}x^k}g_l(x_j)=(\mathbf{D}_k\mathbf{u})_j,$$

where $\mathbf{D}_k$ is an $m\times m$ matrix with elements $(\mathbf{D}_k)_{jl}=\frac{\mathrm{d}^k}{\mathrm{d}x^k}g_l(x_j)$, $j,l=0,1,\cdots,m-1$, and $\mathbf{u}=(u_0,u_1,\cdots,u_{m-1})^T$. According to [36], the following one-order and two-order spectral differential matrices are written explicitly as

$$(\mathbf{D}_1)_{jl}=\begin{cases}\frac{1}{2}\mu(-1)^{j+l}\cot\left(\mu\frac{x_j-x_l}{2}\right), & j\neq l,\\ 0, & j=l,\end{cases}$$

$$(\mathbf{D}_2)_{jl}=\begin{cases}\frac{1}{2}\mu^2(-1)^{j+l+1}\frac{1}{\sin^2(\mu(x_j-x_l)/2)}, & j\neq l,\\ -\mu^2\frac{2(l/2)^2+1}{6}, & j=l.\end{cases}$$

In particular, $\mathbf{D}_1$ and $\mathbf{D}_2$ have the following properties

$$\mathbf{D}_1=\mathbf{F}^H\Lambda_1\mathbf{F},\quad \Lambda_1=\mathrm{i}\mu\mathrm{diag}\Big(0,1,\cdots,\frac{m}{2}-1,0,-\frac{m}{2}+1,\cdots,-1\Big),$$

$$\mathbf{D}_2=\mathbf{F}^H\Lambda_2\mathbf{F},\quad \Lambda_2=\Big[\mathrm{i}\mu\mathrm{diag}\Big(0,1,\cdots,\frac{m}{2}-1,\frac{m}{2},-\frac{m}{2}+1,\cdots,-1\Big)\Big]^2,$$

where $\mathbf{F}$ is the discrete Fourier transform matrix with elements $(\mathbf{F})_{jl}=\frac{1}{\sqrt{m}}\mathrm{e}^{-\mathrm{i}\frac{2\pi}{m}jl}$, $\mathbf{F}^H$ is the conjugate transpose of $\mathbf{F}$, which corresponds to the discrete inverse Fourier transform matrix. From this, it follows that $\mathbf{D}_1$ is a real skew-symmetric matrix, while $\mathbf{D}_2$ is a real symmetric matrix.

For simplicity, when $\mathbf{u}$ and $\mathbf{v}$ are vectors, and $p\in\mathbb{Z}$ we denote

$$\mathbf{uv}=(u_0v_0,\cdots,u_{m-1}v_{m-1})^T,\quad \mathbf{u}/\mathbf{v}=\Big(u_0/v_0,\cdots,u_{m-1}/v_{m-1}\Big),\quad \mathbf{u}^p=(u_0^p,u_1^p,\cdots,u_{m-1}^p)^T.$$

Given two vectors $\mathbf{u}$ and $\mathbf{v}$, we define the discrete norms by

$$(\mathbf{u},\mathbf{v})_h=h\mathbf{v}^H\mathbf{u}=h\sum_{j=0}^{n-1}u_j\bar{v}_j,\quad \|\mathbf{u}\|_h=\sqrt{(\mathbf{u},\mathbf{u})_h}.$$

Denote $v_h(t)$ the approximated solution of $v(t)$, i.e., $v_h \approx v(t)$. Then, the spatial semi-discrete scheme for the system (2.7) reads

$$\begin{cases} \partial_t \mathbf{u} = \mathbf{D}\Big[\frac{\frac{\delta}{\delta \mathbf{u}}(H_h[\mathbf{u}]-M_h[\mathbf{u}])}{\sqrt{M_h[\mathbf{u}]}}\cdot v_h + \frac{\delta M_h[\mathbf{u}]}{\delta \mathbf{u}}\Big] =: f(\mathbf{u},v_h), \\ \frac{\mathrm{d}}{\mathrm{d}t}v_h = -\frac{1}{2}\Big(\frac{\frac{\delta}{\delta \mathbf{u}}(H_h[\mathbf{u}]-M_h[\mathbf{u}])}{\sqrt{M_h[\mathbf{u}]}},\partial_t \mathbf{u}\Big)_h =: g(\mathbf{u},v_h), \end{cases} \tag{4.2}$$

where $H_h[\mathbf{u}]$, $M_h[\mathbf{u}]$ and $H_h[\mathbf{u}_0]$ are expressions obtained through spatial discretization, with specific forms provided in the latter examples in Section 6. $\mathbf{D}$ is a real antisymmetric matrix, which is determined by a skew adjoint operator $\mathcal{D}$. It is worth noting that $\mathbf{u}$ and $f(\mathbf{u},v_h)$ are both $m\times 1$ vectors, and v_h and $g(\mathbf{u},v_h)$ are both scalars.

Denote the spatial semi-discrete mass and energy, respectively, by

$$M_{1,h}[\mathbf{u}] := (\mathbf{u},\mathbf{1})_h, \quad E_h[\mathbf{u},v_h] := -v_h^2 + M_h[\mathbf{u}] + H_h[\mathbf{u}_0]$$

with $\mathbf{1}=(1,1,\cdots,1)^T$. Then we have the following result:

Theorem 4.1. *The semi-discrete scheme* (4.2) *derived from the discretization of the Fourier pseudo-spectral method has the following conservation properties*

$$\frac{\mathrm{d}}{\mathrm{d}t}M_{1,h}[\mathbf{u}] = 0, \quad \frac{\mathrm{d}}{\mathrm{d}t}E_h[\mathbf{u},v_h] = 0.$$

Proof. The proof follows a similar approach to (1.3) or (1.2). Taking an inner product of the first equation in (4.2) with $\mathbf{1}$, and noticing $\mathbf{D1}=\mathbf{0}$, it follows the mass conservation directly. Using the second equation in (4.2), we have

$$\begin{aligned} \frac{\mathrm{d}}{\mathrm{d}t}E_h[\mathbf{u},v_h] &= -2v_h\frac{\mathrm{d}}{\mathrm{d}t}v_h + \Big(\frac{\delta M_h[\mathbf{u}]}{\delta \mathbf{u}},\partial_t \mathbf{u}\Big)_h \\ &= v_h\Big(\frac{\frac{\delta}{\delta \mathbf{u}}(H_h[\mathbf{u}]-M_h[\mathbf{u}])}{\sqrt{M_h[\mathbf{u}]}},\partial_t \mathbf{u}\Big)_h + \Big(\frac{\delta M_h[\mathbf{u}]}{\delta \mathbf{u}},\partial_t \mathbf{u}\Big)_h \\ &= \Big(\frac{\delta H_h[\mathbf{u}]}{\delta \mathbf{u}},\partial_t \mathbf{u}\Big)_h = \Big(\frac{\delta H_h[\mathbf{u}]}{\delta \mathbf{u}},\mathbf{D}\frac{\delta H_h[\mathbf{u}]}{\delta \mathbf{u}}\Big)_h = 0, \end{aligned}$$

where $v_h=\sqrt{M_h[\mathbf{u}]}$ has been used in the third line above and the skew-symmetry of $\mathbf{D}$ is utilized in the second line. □

4.2 Full discretization

We now combine the temporal and spatial discretization to construct the following fully discrete SAV-RK*s* scheme for the system (2.7):

$$\begin{cases} \mathbf{u}^{k+1} = \mathbf{u}^k + \tau\sum_{i=1}^{s} b_i f_i, \quad \mathbf{U}_i = \mathbf{u}^k + \tau\sum_{j=1}^{s} a_{ij} f_j, \\ v_h^{k+1} = v_h^k + \tau\sum_{i=1}^{s} b_i g_i, \quad V_i = v_h^k + \tau\sum_{j=1}^{s} a_{ij} g_j, \end{cases} \tag{4.3}$$

where

$$\begin{cases} f_i = f(\mathbf{U}_i, V_i) = \mathbf{D}\Big[Q_i \cdot V_i + \dfrac{\delta M_h[\mathbf{U}_i]}{\delta \mathbf{U}_i}\Big], \\ g_i = g(\mathbf{U}_i, V_i) = -\dfrac{1}{2}(Q_i, f_i), \\ Q_i = Q[\mathbf{U}_i, V_i] = \dfrac{\frac{\delta}{\delta \mathbf{U}_i}(H_h[\mathbf{U}_i] - M_h[\mathbf{U}_i])}{\sqrt{M_h[\mathbf{U}_i]}} \end{cases}$$

with the initial values given by

$$\mathbf{u}_0 = u_0(\mathbf{x}), \quad v_h^0 = \sqrt{M_h[\mathbf{u}_0]}.$$

We define the discrete mass and energy for the numerical scheme (4.3) as

$$M_{1,h}[\mathbf{u}^k] := (\mathbf{u}^k, \mathbf{1})_h, \quad E_h^k = E_h[\mathbf{u}^k, v_h^k] := -(v_h^k)^2 + M_h[\mathbf{u}^{\mathbf{k}}] + H_h[\mathbf{u}_0].$$

Then, by combining the proofs of Theorem 3.1 and Theorem 4.1, we can easily establish the following result.

Theorem 4.2. *The fully discrete SAV-RKs scheme* (4.3) *conserves the discrete mass and energy, i.e.,*

$$M_{1,h}[\mathbf{u}^k] = M_{1,h}[\mathbf{u}_0], \quad E_h^{k+1} = E_h^k = H_h[\mathbf{u}_0], \quad k = 1, 2, \cdots, n-1.$$

Remark 4.1. The scheme (4.3) is specifically designed for real-valued systems. For complex-valued systems such as NLS, it suffices to replace $g_i = g(\mathbf{U}_i, V_i) = -\frac{1}{2}(Q_i, f_i)$ in (4.3) with $g_i = g(\mathbf{U}_i, V_i) = -\mathrm{Re}(Q_i, f_i)$.

Remark 4.2. Due to the pseudo-spatial discretization, $M_{2,h}^k$ is only preserved up to the spatial discretization error. It is possible to preserve $M_{2,h}^k$ exactly if one uses a pure spectral-Galerkin discretization without numerical quadrature, albeit at a much higher cost.

5 A fast solver

The numerical scheme (4.3) is a coupled nonlinear system. We develop in this section a customized fast solver for (4.3) based on FFT and the Newton's iteration method.

Define

$\mathbf{U} = (\mathbf{U}_1^T, \cdots, \mathbf{U}_s^T)^T \in \mathbb{V}^{ms \times 1}$, $\mathbf{Q} = (Q_1^T, \cdots, Q_s^T)^T \in \mathbb{V}^{ms \times 1}$, $\mathbf{V} = (V_1, \cdots, V_s)^T \in \mathbb{V}^{s \times 1}$,
$\mathbf{g} = (g_1, \cdots, g_s)^T \in \mathbb{V}^{s \times 1}$, $\mathbf{f} = (f_1^T, \cdots, f_s^T)^T \in \mathbb{V}^{ms \times 1}$, $\mathbf{e}_{d \times 1} = (1, 1, \cdots, 1)^T \in \mathbb{V}^{d \times 1}$,
$\mathrm{reshape}(\mathbf{f}) = (f_1, \cdots, f_s) \in \mathbb{V}^{m \times s}$, and $\mathbf{I}_d$ represents the $d \times d$ identity matrix.

Then the system (4.3) can be solved consecutively as follows: Calculate

$$\begin{cases} \mathbf{U}=\mathbf{e}_{s\times 1}\otimes\mathbf{u}^k+(\mathbf{A}\otimes\mathbf{I}_s)\mathbf{f}, \\ \mathbf{P}=\sqrt{M_h[\mathbf{U}]}, \\ \mathbf{Q}=\dfrac{\delta(H_h[\mathbf{U}]-M_h[\mathbf{U}])}{\delta\mathbf{U}}/\big(\mathbf{P}\otimes\mathbf{e}_{m\times 1}\big). \end{cases}$$

Solve the nonlinear system

$$\mathbf{f}=(\mathbf{I}_s\otimes\mathbf{D})\Big[\mathbf{Q}(\mathbf{V}\otimes\mathbf{e}_{m\times 1})+\frac{\delta M_h[\mathbf{U}]}{\delta\mathbf{U}}\Big], \tag{5.1}$$

where

$$\begin{cases} \mathbf{g}=-\dfrac{1}{2}\Big((Q_1,\mathbf{f}_1)_h,\cdots,(Q_s,\mathbf{f}_s)_h\Big)^T, \\ \mathbf{V}=v_h^k+\tau\mathbf{A}\mathbf{g}. \end{cases}$$

Update the solution:

$$\begin{cases} v_h^{k+1}=v_h^k+\tau\mathbf{b}^T\mathbf{g}, \\ \mathbf{u}^{k+1}=\mathbf{u}^k+\tau\cdot\mathrm{reshape}(\mathbf{f})\mathbf{b}. \end{cases}$$

The key step is to solve the nonlinear system (5.1). Below, we propose a customized Newton iteration with a linearized strategy to efficiently solve it. First, we observe

$$\begin{aligned} \mathbf{f}&=(\mathbf{I}_s\otimes\mathbf{D})\left[\frac{\delta M_h[\mathbf{U}]}{\delta\mathbf{U}}+\mathbf{Q}(\mathbf{V}\otimes\mathbf{e}_{m\times 1})\right] \\ &=(\mathbf{I}_s\otimes\mathbf{D})\left[\frac{\delta M_h[\mathbf{U}]}{\delta\mathbf{U}}+\Big(\frac{\delta(H_h[\mathbf{U}]-M_h[\mathbf{U}])}{\delta\mathbf{U}}/\big(\mathbf{P}\otimes\mathbf{e}_{m\times 1}\big)\Big)\big(\mathbf{V}\otimes\mathbf{e}_{m\times 1}\big)\right] \\ &=(\mathbf{I}_s\otimes\mathbf{D})\left[\frac{\delta M_h[\mathbf{U}]}{\delta\mathbf{U}}+\Big(\frac{\delta(H_{L,h}[\mathbf{U}]+H_{N,h}[\mathbf{U}]-M_h[\mathbf{U}])}{\delta\mathbf{U}}/\big(\mathbf{P}\otimes\mathbf{e}_{m\times 1}\big)\Big)\big(\mathbf{V}\otimes\mathbf{e}_{m\times 1}\big)\right] \\ &=(\mathbf{I}_s\otimes\mathbf{D})\left[\frac{\delta M_h[\mathbf{U}]}{\delta\mathbf{U}}+\Big(\frac{\delta(H_{L,h}[\mathbf{U}]-M_h[\mathbf{U}])}{\delta\mathbf{U}}/\big(\mathbf{P}\otimes\mathbf{e}_{m\times 1}\big)\Big)\big(\mathbf{V}\otimes\mathbf{e}_{m\times 1}\big)\right. \\ &\qquad\left.+\Big(\frac{\delta H_{N,h}[\mathbf{U}]}{\delta\mathbf{U}}/\big(\mathbf{P}\otimes\mathbf{e}_{m\times 1}\big)\Big)\big(\mathbf{V}\otimes\mathbf{e}_{m\times 1}\big)\right]. \end{aligned} \tag{5.2}$$

Let $\mathbf{L}$ be the matrix determined by the Fourier pseudo-spectral approximation of the operator $\mathcal{L}$. Thanks to (2.6), we have $\mathbf{P}\approx\mathbf{V}$, so we can approximate the above by

$$\begin{aligned}
\mathbf{f}&\approx(\mathbf{I}_s\otimes\mathbf{D})\left[\frac{\delta H_{L,h}[\mathbf{U}]}{\delta\mathbf{U}}+\left(\frac{\delta H_{N,h}[\mathbf{U}]}{\delta\mathbf{U}}/\left(\mathbf{P}\otimes\mathbf{e}_{m\times1}\right)\right)\left(\mathbf{V}\otimes\mathbf{e}_{m\times1}\right)\right]\\
&=(\mathbf{I}_s\otimes\mathbf{D})\left[(\mathbf{I}_s\otimes\mathbf{L})\mathbf{U}+\left(\frac{\delta H_{N,h}[\mathbf{U}]}{\delta\mathbf{U}}/\left(\mathbf{P}\otimes\mathbf{e}_{m\times1}\right)\right)\left(\mathbf{V}\otimes\mathbf{e}_{m\times1}\right)\right]\\
&=(\mathbf{I}_s\otimes\mathbf{D})\left[(\mathbf{I}_s\otimes\mathbf{L})(\mathbf{e}_{s\times1}\otimes\mathbf{u}^k+\tau(\mathbf{A}\otimes\mathbf{I}_m)\mathbf{f})+\left(\frac{\delta H_{N,h}[\mathbf{U}]}{\delta\mathbf{U}}/\left(\mathbf{P}\otimes\mathbf{e}_{m\times1}\right)\right)\left(\mathbf{V}\otimes\mathbf{e}_{m\times1}\right)\right]\\
&=(\mathbf{I}_s\otimes\mathbf{D})\left[\mathbf{e}_{s\times1}\otimes(\mathbf{L}\mathbf{u}^k)+\tau(\mathbf{A}\otimes\mathbf{L})\mathbf{f}+\left(\frac{\delta H_{N,h}[\mathbf{U}]}{\delta\mathbf{U}}/\left(\mathbf{P}\otimes\mathbf{e}_{m\times1}\right)\right)\left(\mathbf{V}\otimes\mathbf{e}_{m\times1}\right)\right].
\end{aligned}$$

Hence, we can approximate (5.1) by

$$\varphi(\mathbf{f}):=\mathbf{f}-(\mathbf{I}_s\otimes\mathbf{D})\left[\mathbf{e}_{s\times1}\otimes(\mathbf{L}\mathbf{u}^k)+\tau(\mathbf{A}\otimes\mathbf{L})\mathbf{f}+\left(\frac{\delta H_{N,h}[\mathbf{U}]}{\delta\mathbf{U}}/\left(\mathbf{P}\otimes\mathbf{e}_{m\times1}\right)\right)\left(\mathbf{V}\otimes\mathbf{e}_{m\times1}\right)\right]=\mathbf{0}. \tag{5.3}$$

To this end, we calculate the Jacobian matrix of (5.3) as

$$J_\varphi(\mathbf{f}):=\frac{\partial\varphi(\mathbf{f})}{\partial\mathbf{f}}=\mathbf{I}_{sm}-(\mathbf{I}_s\otimes\mathbf{D})(\tau\mathbf{A}\otimes\mathbf{L})=\mathbf{I}_{sm}-\tau\mathbf{A}\otimes(\mathbf{D}\mathbf{L}).$$

Then, the Newton's iteration method for (5.3) is

$$\mathbf{f}^{l+1}=\mathbf{f}^l-[J_\varphi(\mathbf{f}^l)]^{-1}\varphi(\mathbf{f}^l)=\mathbf{f}^l-[\mathbf{I}_{sm}-\tau\mathbf{A}\otimes(\mathbf{D}\mathbf{L})]^{-1}\varphi(\mathbf{f}^l), \tag{5.4}$$

where $[\mathbf{I}_{sm}-\tau\mathbf{A}\otimes(\mathbf{D}\mathbf{L})]^{-1}$ is a dense matrix of size $sm\times sm$ in (5.4), and the initial guess is $\mathbf{f}^0=\mathbf{e}_{s\times1}\otimes f(\mathbf{u}^k,v_h^k)$.

Remark 5.1. We emphasize that the Jacobian matrix $J_\varphi(\mathbf{f})$ is invariant at each iteration step due to the linearized technique in (5.2). Hence, the iteration can be carried out efficiently using FFT.

6 Numerical results

In this section we carry out numerical simulations on different Hamiltonian systems to evaluate the scheme's performance in terms of accuracy, conservation and computational efficiency. For comparison, we choose the following schemes (with spatial derivatives discretized by the Fourier pseudo-spectral method in all cases):

- SAV-CN [25]: SAV approach combined with the Crank-Nicolson method for time discretization, which is solved by the nonlinear solver presented in this paper.

- SAV-IE [1]: SAV approach combined with a second-order implicit-explicit scheme for time discretization.
- IEQ-RK*s* [50]: IEQ approach combined with the Runge–Kutta method for time discretization.

In all examples below, we set $M[u]=(u,u)$. All numerical experiments are carried out on a 64 bit i5-12500H computer.

For simplicity, we denote the numerical errors and the corresponding numerical convergence orders between the exact solutions and approximate solutions as follows

$$E_\infty(h,\tau)=\max_k\|\mathbf{u}^k-\mathbf{u}(\cdot,t_k)\|_\infty,\quad \mathrm{Ord}_\infty^\tau=\frac{\log_2[E_\infty(h,\tau_1)/E_\infty(h,\tau_2)]}{\log_2(\tau_1/\tau_2)}.$$

To carry out the solution procedure, it is necessary to compute the following quantities:

$$\mathbf{D},\ M_h[\mathbf{u}],\ H_h[\mathbf{u}],\ \frac{\delta M_h[\mathbf{u}]}{\delta\mathbf{u}},\ \frac{\delta H_h[\mathbf{u}]}{\delta\mathbf{u}},\tag{6.1}$$

which are provided in each of the example below.

6.1 Korteweg–de Vries (KdV) equation

For the KdV equation (2.1), the quantities in (6.1) are given by

$$\begin{aligned}&\mathbf{D}=\mathbf{D}_1,\quad M_h[\mathbf{u}]=(\mathbf{u},\mathbf{u})_h,\\&H_h[\mathbf{u}]:=-\frac{1}{2}(\mathbf{u},\mathbf{D}_2\mathbf{u})_h-\frac{1}{6}(\mathbf{u}^3,\mathbf{1})_h,\\&\frac{\delta M_h[\mathbf{u}]}{\delta\mathbf{u}}=2\mathbf{u},\quad \frac{\delta H_h[\mathbf{u}]}{\delta\mathbf{u}}=-\mathbf{D}_2\mathbf{u}-\frac{1}{2}\mathbf{u}^2.\end{aligned}$$

We also have

$$M_{1,h}^k=M_{1,h}[\mathbf{u}^k]:=(\mathbf{u}^k,\mathbf{1})_h,\tag{6.2}$$
$$M_{2,h}^k=M_{2,h}[\mathbf{u}^k]:=(\mathbf{u}^k,\mathbf{u}^k)_h,\tag{6.3}$$
$$H_h^k=H_h[\mathbf{u}^k]:=-\frac{1}{2}(\mathbf{u}^k,\mathbf{D}_2\mathbf{u}^k)_h-\frac{1}{6}((\mathbf{u}^k)^3,\mathbf{1})_h,\tag{6.4}$$
$$E_h^k=E_h[\mathbf{u}^k,v_h^k]:=-(v_h^k)^2+M_h[\mathbf{u}^k]+H_h[\mathbf{u}_0].\tag{6.5}$$

Example 6.1. We consider the interaction of two-soliton solutions satisfying the problem (2.1) [47]. The exact solution is

$$u(x,t+T/2)=12\frac{\gamma_1^2e^{\theta_1}+\gamma_2^2e^{\theta_2}+2(\gamma_2-\gamma_1)^2e^{\theta_1+\theta_2}+a^2(\gamma_2^2e^{\theta_1}+\gamma_1^2e^{\theta_2})e^{\theta_1+\theta_2}}{(1+e^{\theta_1}+e^{\theta_2}+a^2e^{\theta_1+\theta_2})^2},$$

Table 1: The numerical errors, convergence rates and CPU time of SAV-IE and SAV-RKs with $h=0.02$ and $\tau=T/n$ in Example 6.1.

Schemes	SAV-IE	SAV-RK1	SAV-RK2	SAV-RK3	SAV-RK4	n
$E_\infty(h,\tau)$	2.8787e−03	1.6007e−04	1.2484e−07	1.0149e−09	1.0365e−11	16
	1.8266e−03	1.0246e−04	4.9882e−08	2.4659e−10	1.9824e−12	20
	1.2623e−03	7.1158e−05	2.3755e−08	7.5090e−11	4.8683e−13	24
	9.2462e−04	5.2281e−05	1.2731e−08	2.8839e−11	1.4355e−13	28
	7.0647e−04	4.0028e−05	7.4298e−09	1.2585e−11	4.9183e−14	32
	5.5738e−04	3.1627e−05	4.6247e−09	6.0448e−12	2.0206e−14	36
Ord_∞^τ	–	–	–	–	–	16
	2.0385	1.9992	4.1111	6.3403	7.4130	20
	2.0265	1.9999	4.0690	6.5216	7.7015	24
	2.0197	1.9998	4.0463	6.2079	7.9223	28
	2.0152	1.9999	4.0332	6.2098	8.0217	32
	2.0124	1.9999	4.0250	6.2261	7.5526	36
CPU time	0.1523	0.2289	0.3623	0.5163	0.6519	16
	0.1649	0.2636	0.4170	0.5959	0.7715	20
	0.1841	0.3016	0.4816	0.6448	0.9006	24
	0.2177	0.3263	0.5291	0.7304	0.9710	28
	0.2348	0.3694	0.5981	0.7787	1.0711	32
	0.2496	0.3934	0.6286	0.8468	1.2114	36

where the parameters are selected as

$$\gamma_1=0.4,\quad \gamma_2=0.6,\quad a^2=\left(\frac{\gamma_1-\gamma_2}{\gamma_1+\gamma_2}\right)^2=\frac{1}{25},$$
$$\theta_1=\gamma_1 x-\gamma_1^3 t+x_1,\quad \theta_2=\gamma_2 x-\gamma_2^3 t+x_2,\quad x_1=10,\quad x_2=25.$$

For this first example, we provide detailed numerical results and comparisons in Table 1 and Figs. 2-5.

- We select the computational domain $\Omega=[-100,100]$ and a terminal time $T=8$. Fixing the spatial partition number $m=10^4$, we observe from Table 1 that the convergence rates of the s-stage Gaussian Runge–Kutta method indeed achieves order $2s$, and that the CPU time of our nonlinear scheme using the fast solver is slightly more than the implicit-explicit linear scheme (SAV-IE) but offers much higher accuracy.

- Fig. 1 demonstrates that the iteration numbers remain nearly constant when the temporal step sizes are fixed. Moreover, it also reveals that the iteration numbers are largely independent of the stages of the Runge–Kutta methods but strongly

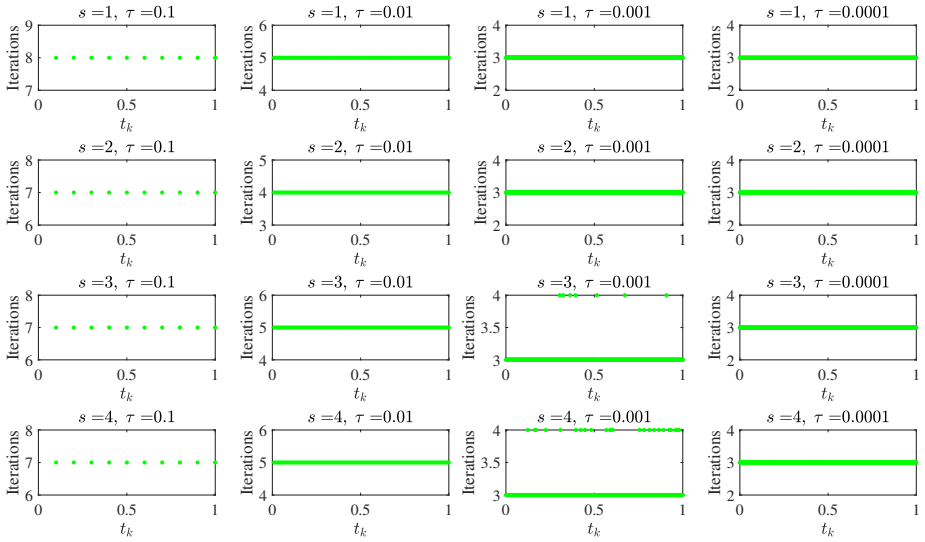

Figure 1: The iteration numbers versus the time step sizes and Runge–Kutta stages in Example 6.1.

depends on the temporal step size. Specifically, smaller time step sizes result in fewer iterations.

- Conservation properties of $M_{1,h}^k$, $M_{2,h}^k$, E_h^k and H_h^k are shown in Fig. 2. We observe that M_{1,h^k}, $M_{2,h}^k$ and E_h^k are conserved in the discrete sense with the SAV-RKs scheme. However, the SAV-IE scheme only conserves the Hamiltonian energy E_h^k.

- In Fig. 3, we use the SAV-RK3 scheme to compare conservation with IEQ-RKs and SAV-CN schemes for the discrete quantities $M_{1,h}^k$, $M_{2,h}^k$, E_h^k and H_h^k. We choose $\Omega=[-100,100]$, $T=200$ and $h=\tau=0.02$. It is obvious that schemes IEQ-RK1 and SAV-CN manifest the worst conservation effect. Our scheme SAV-RK3 has the best conservation effect. In addition, we observe that the high-order IEQ-RK4 scheme also has better performance since the numerical error $|E_h^k-H_h^0|$ remains at the 10^{-15} level. However, after $t>60$ approximately, the numerical error $|E_h^k-H_h^0|$ of IEQ-RK4 scheme starts to accumulate and decrease to 10^{-12} level, which is worse than SAV-RK3 scheme.

- Fig. 4 shows the numerical solution by using SAV-RK3 over time interval $t\in[0,200]$. The numerical solutions at $t_k=0$, 25, 100 and 175 are plotted in Fig. 5. Note that the initial condition $u(x,0)$ consists of two solitons: one with a higher amplitude and the other with a lower amplitude. As time evolves, the higher one catches up with the lower one, gradually causing a collision. Subsequently, two solitons separate from each other and continue to propagate independently over time.

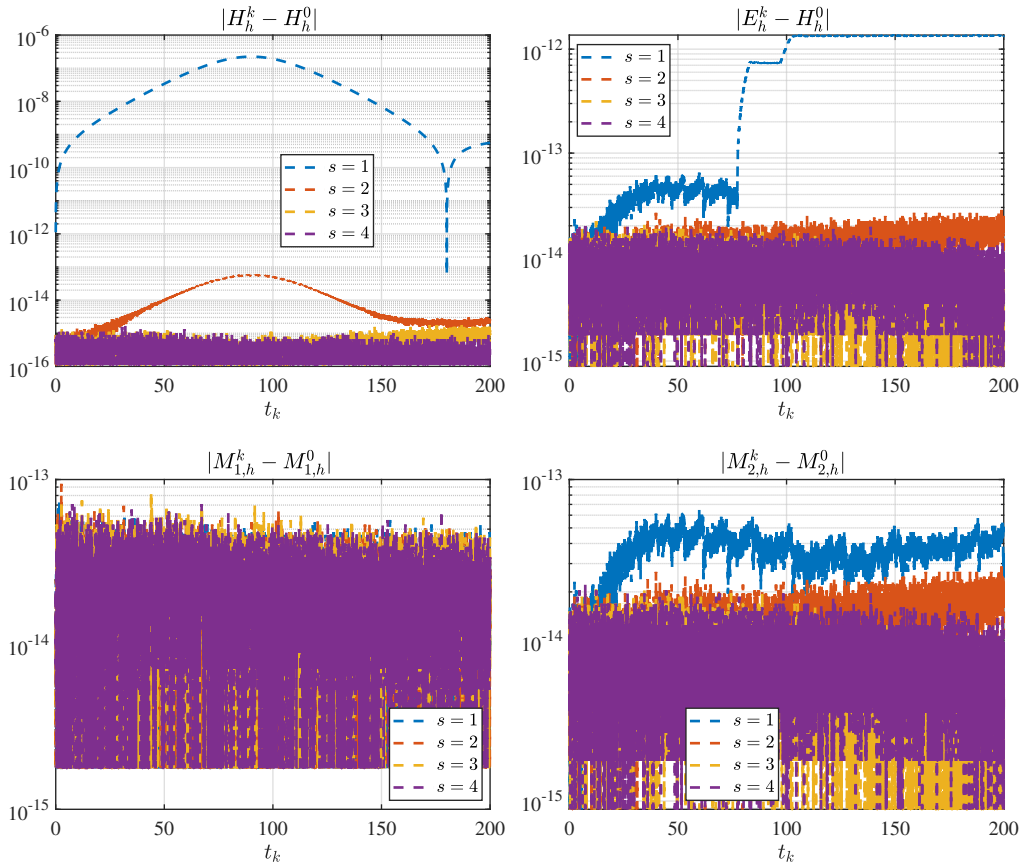

Figure 2: Numerical errors of discrete conservative quantities (6.2)-(6.5) with SAV-RKs in Example 6.1, where $h=\tau=0.02$.

6.2 Nonlinear Schrödinger (NLS) equation

For the NLS equation (2.2), the quantities in (6.1) read

$$\begin{aligned}
&\mathbf{D}=-\mathrm{i}\mathbf{I}_m, \quad M_h[\mathbf{u}]=(\mathbf{u},\mathbf{u})_h,\\
&H_h[\mathbf{u}]:=-(\mathbf{u},\mathbf{D}_2\mathbf{u})_h-(\mathbf{u}^2,\mathbf{u}^2)_h,\\
&\frac{\delta M_h[\mathbf{u}]}{\delta\bar{\mathbf{u}}}=\mathbf{u}, \quad \frac{\delta H_h[\mathbf{u}]}{\delta\bar{\mathbf{u}}}=-\mathbf{D}_2\mathbf{u}-2|\mathbf{u}|^2\mathbf{u}.
\end{aligned}$$

In addition,

$$M_{2,h}^k=M_{2,h}[\mathbf{u}^k]:=(\mathbf{u}^k,\mathbf{B}\mathbf{u}^k)_h, \quad \mathbf{B}=\mathbf{I}_m \text{ or } -\mathrm{i}\mathbf{D}_1, \tag{6.6}$$

$$H_h^k=H_h[\mathbf{u}^k]:=-(\mathbf{u}^k,\mathbf{D}_2\mathbf{u}^k)-((\mathbf{u}^k)^2,(\mathbf{u}^k)^2), \tag{6.7}$$

$$E_h^k=E_h[\mathbf{u}^k,v_h^k]:=-(v_h^k)^2+M_h[\mathbf{u}^k]+H_h[\mathbf{u}_0]. \tag{6.8}$$

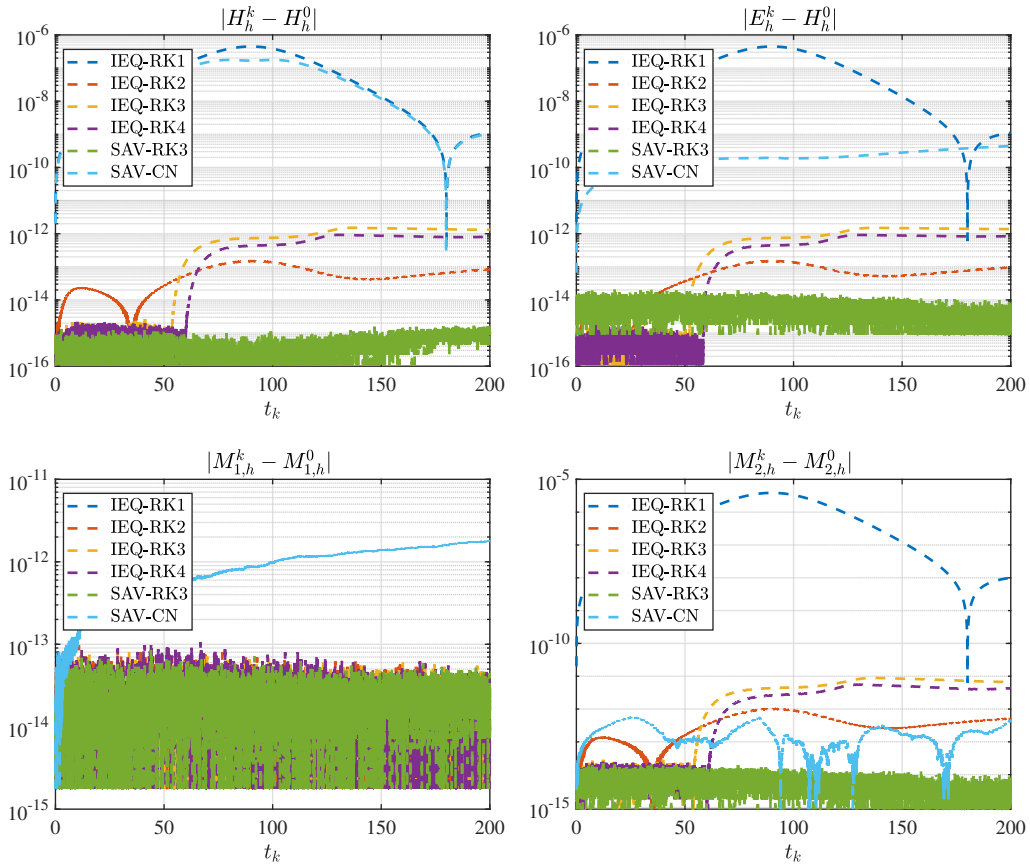

Figure 3: Numerical errors of discrete quantities calculated by IEQ-RKs, SAV-RK3 and SAV-CN with $h=\tau=1/100$ over the time interval $t\in[0,200]$ in Example 6.1.

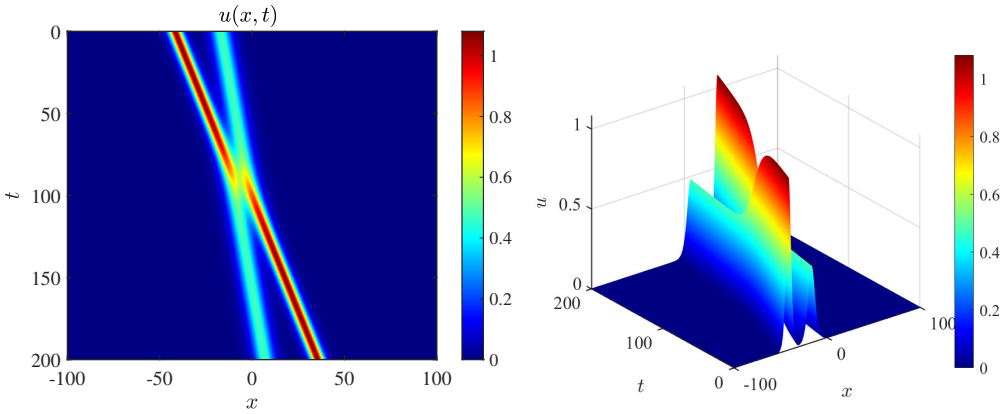

Figure 4: Evolution of the numerical solution by SAV-RK3 with $h=\tau=\frac{1}{50}$ in Example 6.1.

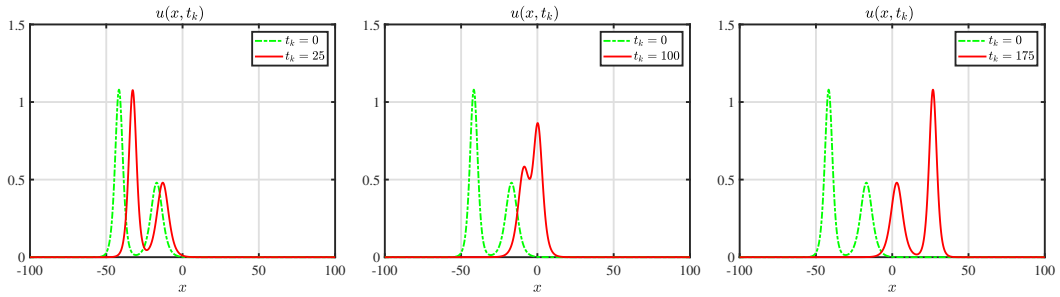

Figure 5: Snapshots of the numerical solution by SAV-RK3 with $h=\tau=0.02$ in Example 6.1; Green line denotes snapshot at $t=0$.

Example 6.2. Consider problem (2.2) with a single-soliton solution from [42]

$$u(x,t+T/2)=\sqrt{\alpha}\mathrm{e}^{\frac{\mathrm{i}}{2}cx-\mathrm{i}(\frac{1}{4}c^2-\alpha)t}\mathrm{sech}(\sqrt{\alpha}(x-ct)),$$

where $\alpha=1$, $c=0.25$ and the domain $\Omega=[-50,50]$.

We set $T=100$ and $m=n=10^4$. We observe from Fig. 6 that the SAV-RKs schemes ($s=2,3,4$) preserve E_h^k exceptionally well, maintaining errors at the 10^{-15} level. Additionally, they conserve $M_{2,h}^k$, and $H_h[\mathbf{u}_0]$ with $\mathbf{B}=\mathbf{I}_m$ or $-\mathrm{i}\mathbf{D}_1$. In contrast, the second-order implicit-explicit scheme fails to preserve $M_{2,h}^k$, and $H_h[\mathbf{u}_0]$, except for E_h^k.

In Figs. 7 and 8, we present the numerical solution over the time interval $[0,100]$. We observe that the initial value $|u_0(x)|$ consists of a single soliton, which propagates smoothly up to $t_k=100$, and the peak of the soliton remains unchanged throughout the entire process.

According to one of the referees' helpful advice, we supplement numerical test for a two-dimensional (2D) NLS equation in the form of

$$\mathrm{i}\partial_t u+(\partial_x^2+\partial_y^2)u+|u|^2u=0$$

with the following initial data.

- **Case I**: $u(x,y,0)=\frac{2}{\sqrt{\pi}}\mathrm{e}^{-(x^2+y^2)}$, see, e.g., [11];
- **Case II**: $u(x,y,0)=(1+\sin x)(2+\sin y)$, see, e.g., [13,28,46].

Case I: The computational domain is chosen as $(x,y,t)\in[-10,10]\times[-10,10]\times[0,10]$. Numerical surfaces of the 2D NLS equation are conducted using the SAV-RK3 scheme, and the numerical results using the SAV-RKs schemes are shown in Fig. 9, which are consistent with those in [11]. The discrete conservation laws are also preserved very well.

Case II: The computational domain is chosen as $(x,y,t)\in[0,2\pi]\times[0,2\pi]\times[0,0.2]$. Numerical surfaces of the 2D NLS equation are conducted using the SAV-RK2 scheme, and

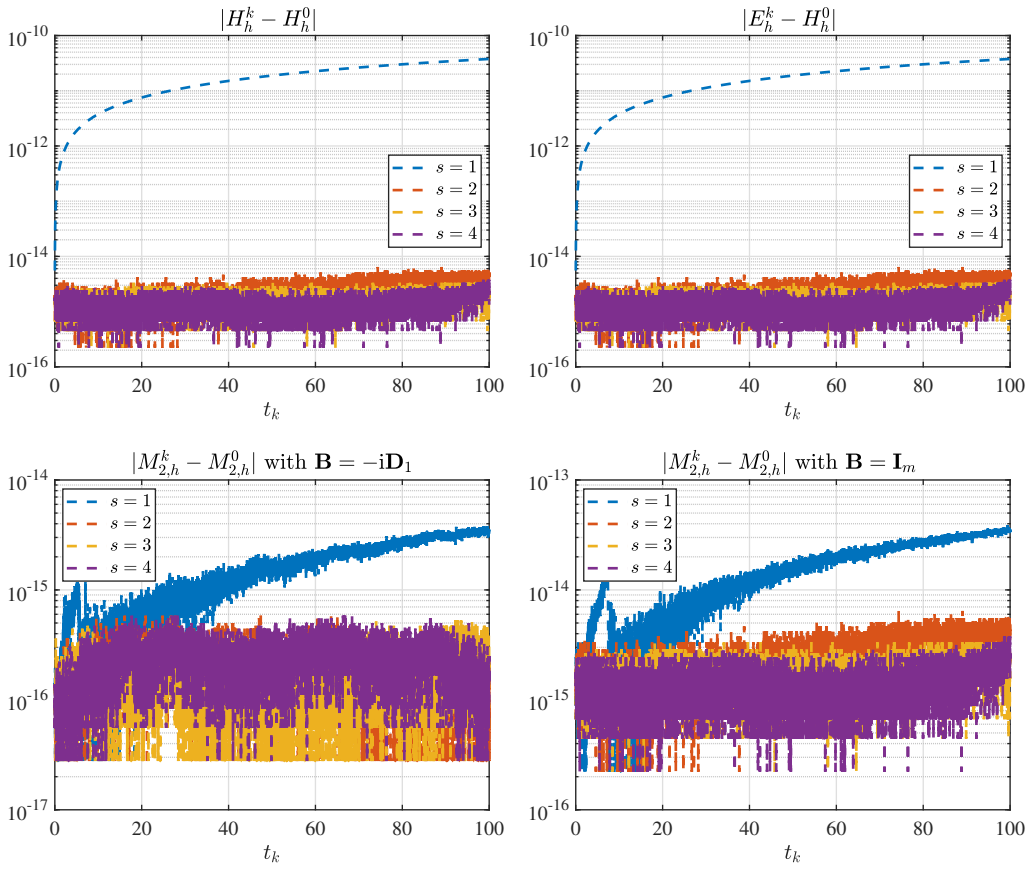

Figure 6: Numerical errors of discrete conservative quantities (6.6)-(6.8) with SAV-RKs in Example 6.2, where $h=\tau=0.01$.

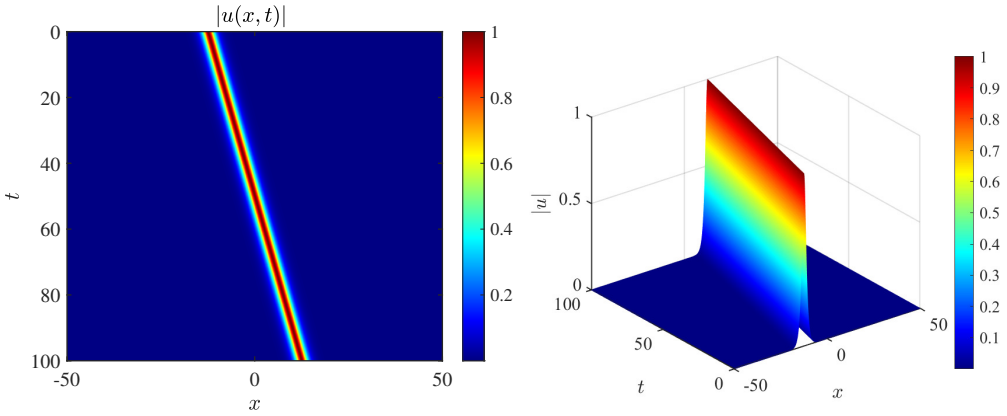

Figure 7: Evolution of the numerical solution in Example 6.2 from SAV-RK3 with $h=\tau=0.01$.

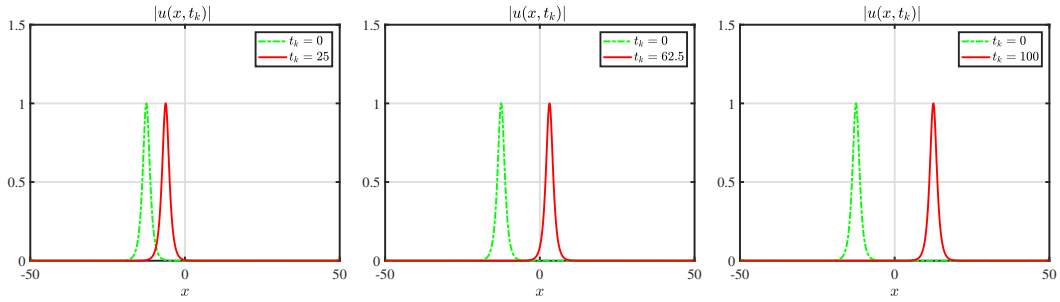

Figure 8: Snapshots of the numerical solution by SAV-RK3 with $h=\tau=0.01$ in Example 6.2; Green line denotes snapshot at $t=0$.

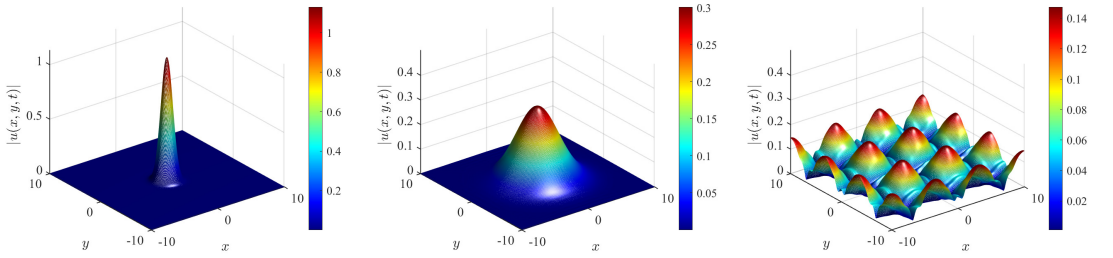

(a) $t=0$ (b) $t=1$ (c) $t=10$

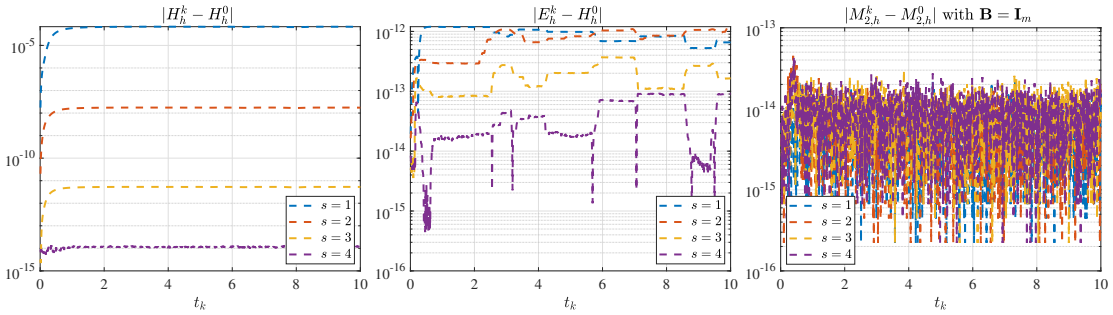

(d) (e) (f)

Figure 9: Initial data in **Case I** for 2D NLS equation with the step sizes $h=20/256$ and $\tau=1/100$: (a)-(c) denote snapshots of numerical solutions calculated by SAV-RK3; (d)-(f) denote the numerical errors of the discrete conserved quantities by using SAV-RKs.

numerical conservation laws are displayed in Fig. 10, which are in nice agreement with those in [13,28,46]. The numerical errors of the discrete conservation laws are very small, even though the problem has a singular solution. It is worth noting that due to the non-smoothness of the problem, the performance of higher-order RKs schemes is worse than that of lower-order ones. Therefore, we select RK2 for the simulation in Fig. 10(a)-(c).

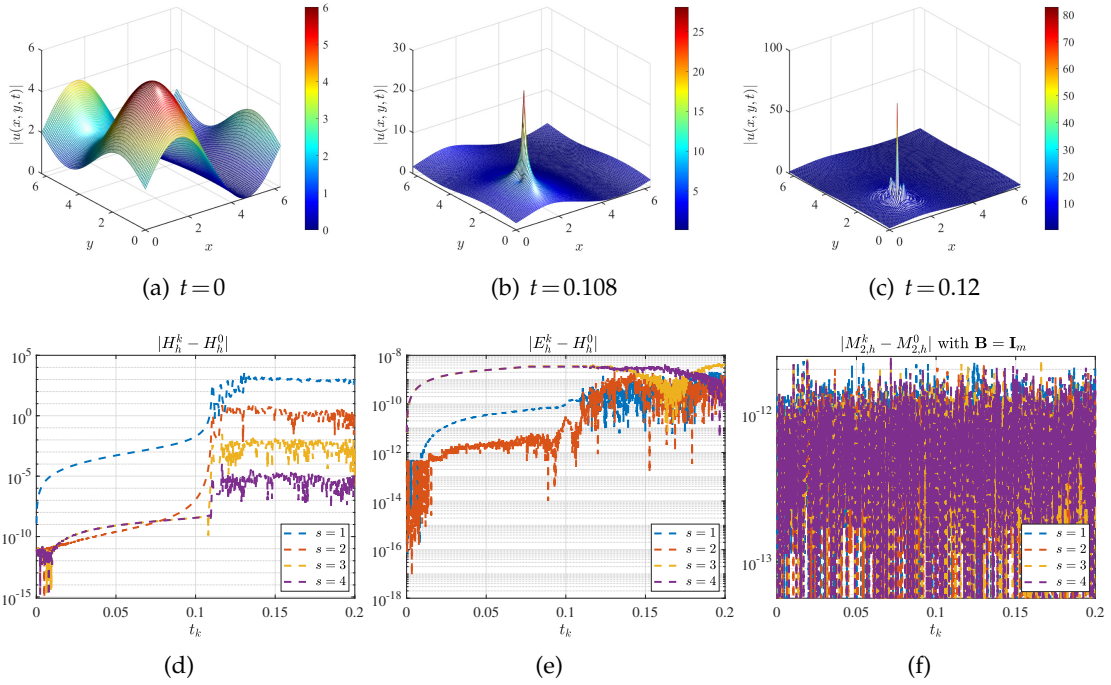

Figure 10: Initial data in **Case II** for 2D NLS equation with the step sizes $h=2\pi/128$ and $\tau=1/10000$: (a)-(c) denote snapshots of numerical solutions calculated by SAV-RK2; (d)-(f) denote the numerical errors of the discrete conserved quantities by using SAV-RKs.

6.3 First-type derivative nonlinear Schrödinger (DNLSI) equation

For the DNLSI equation (2.3), (6.1) reads

$$\begin{aligned}
&\mathbf{D}=-\mathbf{D}_1, \quad M_h[\mathbf{u}]=(\mathbf{u},\mathbf{u})_h,\\
&H_h[\mathbf{u}]:=\mathrm{i}(\mathbf{u},\mathbf{D}_1\mathbf{u})_h+\frac{1}{2}(\mathbf{u}^2,\mathbf{u}^2)_h,\\
&\frac{\delta M_h[\mathbf{u}]}{\delta\bar{\mathbf{u}}}=\mathbf{u}, \quad \frac{\delta H_h[\mathbf{u}]}{\delta\bar{\mathbf{u}}}=-\mathrm{i}\mathbf{D}_1\mathbf{u}+|\mathbf{u}|^2\mathbf{u}.
\end{aligned}$$

In addition,

$$M_{1,h}^k=M_{1,h}[\mathbf{u}^k]:=(\mathbf{u}^k,\mathbf{1})_h, \tag{6.9}$$

$$M_{2,h}^k=M_{2,h}[\mathbf{u}^k]:=(\mathbf{u}^k,\mathbf{u}^k)_h, \tag{6.10}$$

$$H_h^k=H_h[\mathbf{u}^k]:=\mathrm{i}(\mathbf{u}^k,\mathbf{D}_1\mathbf{u}^k)_h+\frac{1}{2}((\mathbf{u}^k)^2,(\mathbf{u}^k)^2)_h, \tag{6.11}$$

$$E_h^k=E_h[\mathbf{u}^k,v_h^k]:=-(v_h^k)^2+M_h[\mathbf{u}^k]+H_h[\mathbf{u}_0]. \tag{6.12}$$

Example 6.3. Consider a periodic intersecting two-soliton solution arising from the DNLSI equation (2.3) on the domain $\Omega=[-100,100]$ (see, e.g., [14]) of the form

$$u(x,t+T/2)=W_1\cdot\frac{\bar{W}_2}{W_2^2},$$

where

$$\begin{aligned}
W_1=&\mathrm{e}^{1+(-\frac{1}{20}+\frac{99}{400}\mathrm{i})t+(\frac{1}{2}+\frac{\mathrm{i}}{20})x}+\mathrm{e}^{1+(-\frac{1}{10}+\frac{399}{400}\mathrm{i})t+(1+\frac{\mathrm{i}}{20})x}\\
&-\frac{\mathrm{i}}{8}\Big[\Big(\frac{2}{9}-\frac{\mathrm{i}}{45}\Big)\mathrm{e}^{3+(-\frac{1}{5}+\frac{399}{400}\mathrm{i})t+(2+\frac{\mathrm{i}}{20})x}+\Big(\frac{1}{9}-\frac{\mathrm{i}}{180}\Big)\mathrm{e}^{3+(-\frac{1}{4}+\frac{99}{400}\mathrm{i})t+(\frac{5}{2}+\frac{\mathrm{i}}{20})x}\Big],\\
W_2=&1+\Big(-\frac{1}{40}+\frac{\mathrm{i}}{4}\Big)\mathrm{e}^{x-\frac{t}{10}+2}+\Big(-\frac{1}{160}+\frac{\mathrm{i}}{8}\Big)\mathrm{e}^{2x-\frac{t}{5}+2}\\
&+\Big(-\frac{1}{90}+\frac{\mathrm{i}}{9}\Big)\mathrm{e}^{\frac{3}{2}x+2+t(-\frac{3}{20}-\frac{3}{4}\mathrm{i})}+\Big(-\frac{1}{90}+\frac{2}{9}\mathrm{i}\Big)\mathrm{e}^{\frac{3}{2}x+2+(-\frac{3}{20}t+\frac{3}{4}\mathrm{i})}\\
&+\Big(-\frac{3540607707048805}{9223372036854775808}-\frac{\mathrm{i}}{17280}\Big)\mathrm{e}^{3x-\frac{3t}{10}+4}.
\end{aligned}$$

Numerical results for the DNLSI equation using the SAV-RKs schemes are presented in Figs. 11-13. We observe that the conservation behaviors in Figs. 11 are similar to those for the DNLSII equation. Numerical solutions exhibiting interactions of solitary waves are presented in Figs. 12-13.

6.4 Second-type derivative nonlinear Schrödinger (DNLSII) equation

For the DNLSII equation (2.4), (6.1) reads

$$\begin{aligned}
&\mathbf{D}=-\mathrm{i}\mathbf{I}_m,\quad M_h[\mathbf{u}]=(\mathbf{u},\mathbf{u})_h,\\
&H_h[\mathbf{u}]:=-(\mathbf{u},\mathbf{D}_2\mathbf{u})_h+\frac{\mathrm{i}}{4}(\mathbf{D}_1\mathbf{u}^2,\mathbf{u}^2)_h,\\
&\frac{\delta M_h[\mathbf{u}]}{\delta\bar{\mathbf{u}}}=\mathbf{u},\quad \frac{\delta H_h[\mathbf{u}]}{\delta\bar{\mathbf{u}}}=-\mathbf{D}_2\mathbf{u}+\frac{\mathrm{i}}{2}\bar{\mathbf{u}}(\mathbf{D}_1\mathbf{u}^2).
\end{aligned}$$

We also have

$$M_{2,h}^k=M_{2,h}[\mathbf{u}^k]:=(\mathbf{u}^k,\mathbf{B}\mathbf{u}^k)_h,\quad \mathbf{B}=\mathbf{I}_m\text{ or}-\mathrm{i}\mathbf{D}_1, \tag{6.13}$$

$$H_h^k=H_h[\mathbf{u}^k]:=-(\mathbf{u}^k,\mathbf{D}_2\mathbf{u}^k)_h+\frac{\mathrm{i}}{4}(\mathbf{D}_1(\mathbf{u}^k)^2,(\mathbf{u}^k)^2)_h, \tag{6.14}$$

$$E_h^k=E_h[\mathbf{u}^k,v_h^k]:=-(v_h^k)^2+M_h[\mathbf{u}^k]+H_h[\mathbf{u}_0]. \tag{6.15}$$

Example 6.4. Consider the problem (2.4) with a smooth two-soliton solution derived from [52]

$$u(x,t+T/2)=W_1/W_2,$$

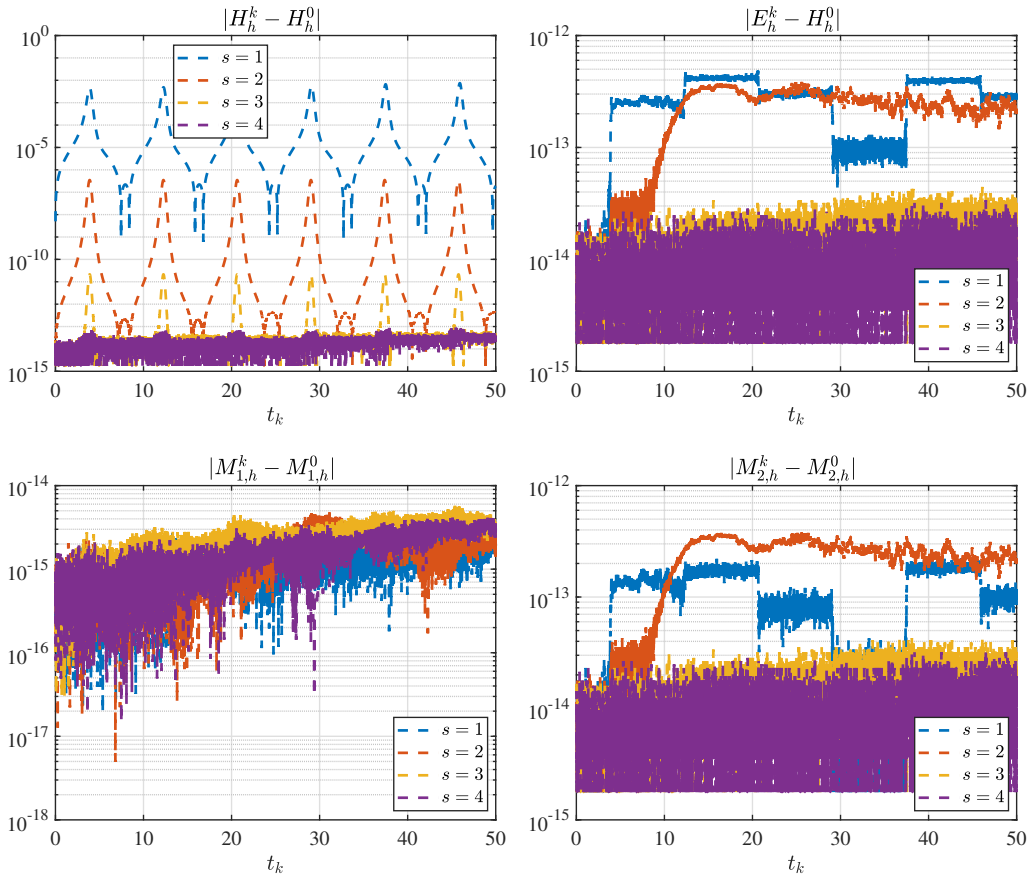

Figure 11: Numerical errors of discrete conservative quantities (6.9)-(6.12) with SAV-RKs in Example 6.3, where $h=0.02$ and $\tau=0.0025$.

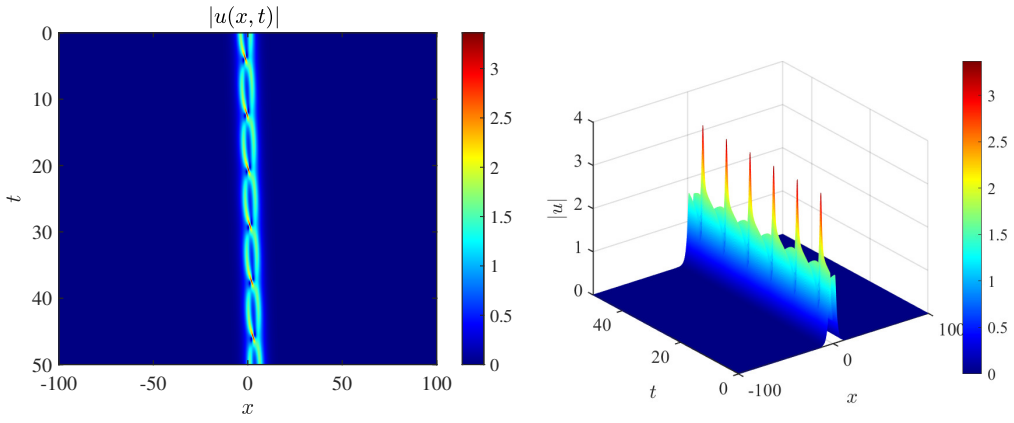

Figure 12: Evolution of the numerical solutions by SAV-RK3 in Example 6.3.

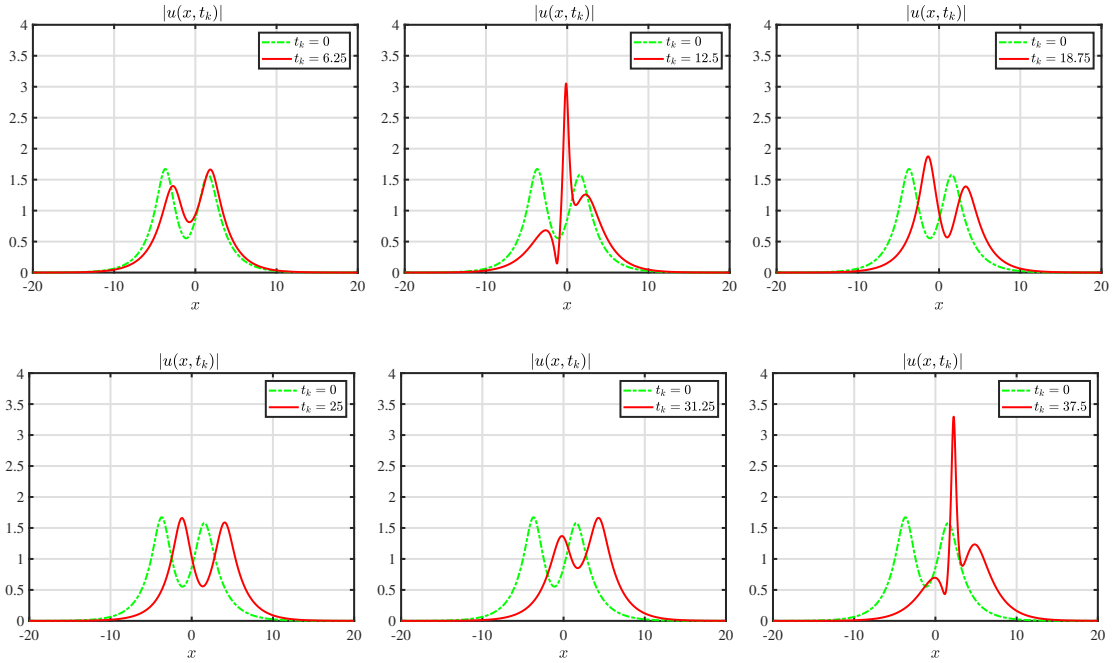

Figure 13: Snapshots of two-soliton solution by SAV-RK3 with $h=0.02$ and $\tau=0.0025$ at t_k in Example 6.3; Green line denotes snapshot at $t=0$.

where

$$
\begin{aligned}
W_1 =& 84\mathrm{i}\Big[(279+28\mathrm{i})\mathrm{e}^{\frac{9}{25}x+\frac{81\mathrm{i}}{625}t}+(-279+28\mathrm{i})\mathrm{e}^{\frac{33}{25}x+(\frac{168}{625}+\frac{81}{625}\mathrm{i})t}\\
&+(316+28\mathrm{i})\mathrm{e}^{(\frac{84}{625}+\frac{527}{2500}\mathrm{i})+(\frac{6}{5}-\frac{7}{50}\mathrm{i})x}+(-316+28\mathrm{i})\mathrm{e}^{(\frac{84}{625}+\frac{527}{2500}\mathrm{i})+(\frac{12}{25}-\frac{7}{50}\mathrm{i})x}\Big],\\
W_2 =& 5\Big[(12691+1813\mathrm{i})\mathrm{e}^{\frac{18}{25}x}+(12691-1813\mathrm{i})\mathrm{e}^{\frac{168}{625}t+\frac{24}{25}x}+(85+595\mathrm{i})\mathrm{e}^{\frac{168}{625}t+\frac{42}{25}x}\\
&-10368\mathrm{e}^{(\frac{84}{625}-\frac{203}{2500}\mathrm{i})t+(\frac{21}{25}+\frac{7}{50}\mathrm{i})x}-14400\mathrm{e}^{(\frac{84}{625}+\frac{203}{2500}\mathrm{i})t+(\frac{21}{25}-\frac{7}{50}\mathrm{i})x}+85-595\mathrm{i}\Big].
\end{aligned}
$$

We choose $\Omega=[-100,100]$, $T=200$, and $m=n=10^4$. We plot in Fig. 14 errors of SAV-RK*s* schemes for the conserved quantities. We observe that all the SAV-RK*s* schemes preserve very well the modified energy E_h^k, $M_{1,h}^k$ and $M_{2,h}^k$. However, preservation of the original energy H_h^k depends on the spatial and time discretization errors.

Fig. 15 further illustrates the numerical solution $|u|$ over the time interval $[0,200]$. Fig. 16 displays the snapshots of the solitary wave at specific time points t_k. Notably, at $t_k=100$, the intersection of two solitary waves generates a sharp peak.

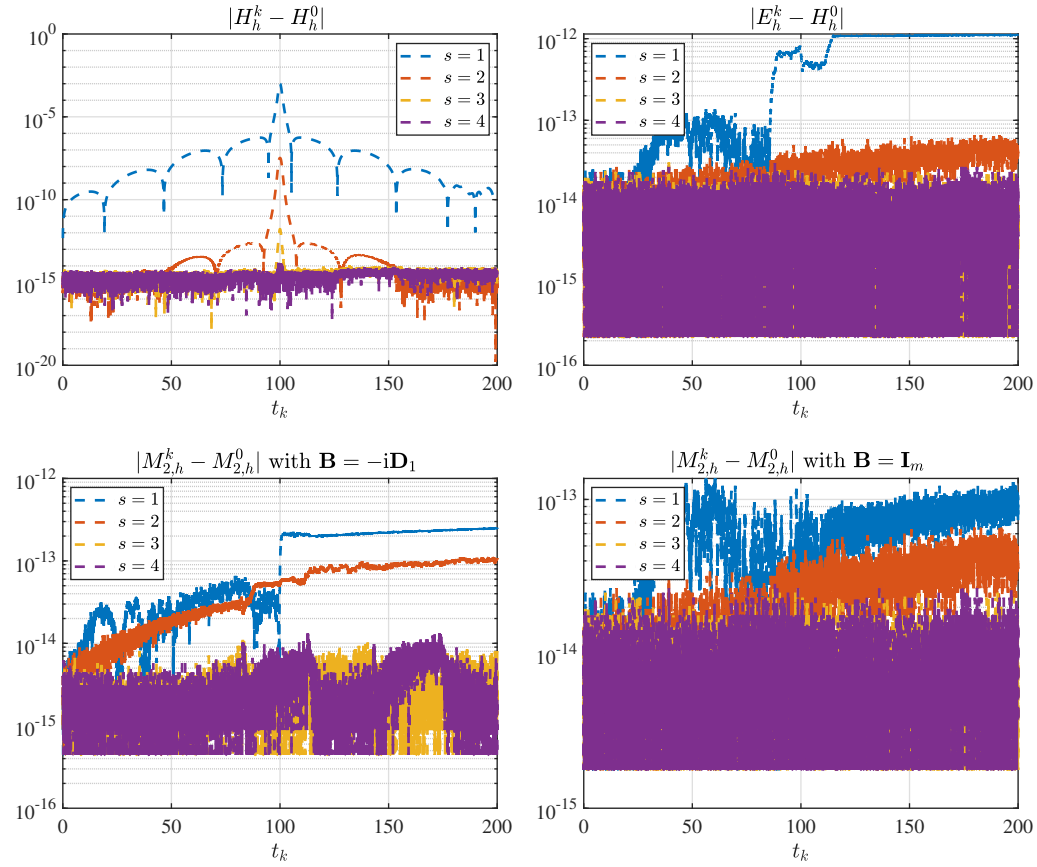

Figure 14: Numerical errors of discrete conservative quantities (6.13)-(6.15) with SAV-RKs in Example 6.4, where $h = \tau = 0.02$.

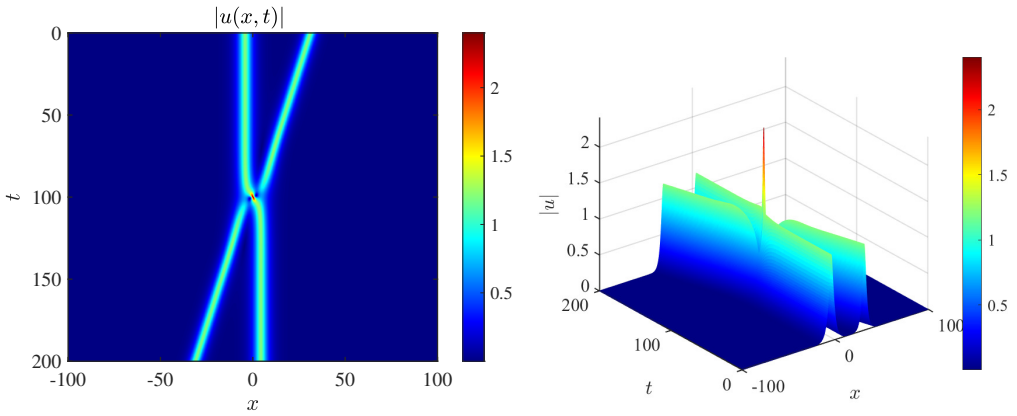

Figure 15: The numerical surfaces by SAV-RK3 in Example 6.4.

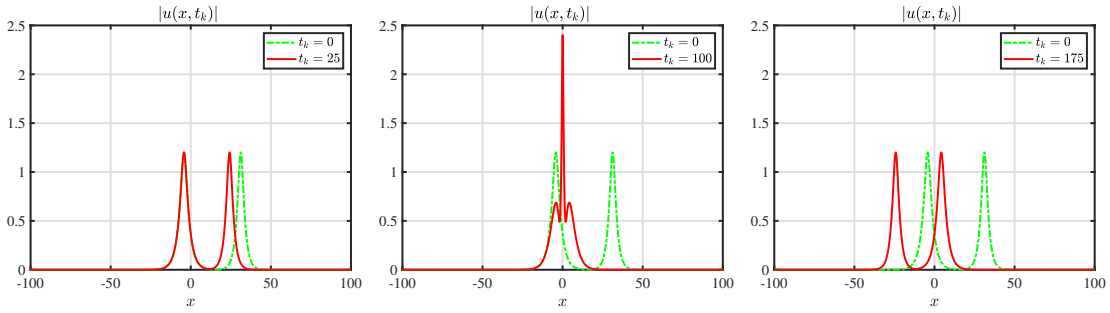

Figure 16: Snapshots of two-soliton solution by SAV-RK3 with $h=\tau=0.02$ in Example 6.4; Green line denotes snapshot at $t=0$.

6.5 Camassa–Holm (CH) equation

For the CH equation, (6.1) reads

$$\begin{aligned}
&\mathbf{D}=(\mathbf{I}_m-\mathbf{D}_2)^{-1}\mathbf{D}_1, \quad M_h[\mathbf{u}]=(\mathbf{u},\mathbf{u})_h,\\
&H_h[\mathbf{u}]:=-\frac{1}{2}(\mathbf{u},\mathbf{u}^2+(\mathbf{D}_1\mathbf{u})^2)_h,\\
&\frac{\delta M_h[\mathbf{u}]}{\delta \mathbf{u}}=2\mathbf{u}, \quad \frac{\delta H_h[\mathbf{u}]}{\delta \mathbf{u}}=-\frac{3}{2}\mathbf{u}^2+\frac{1}{2}(\mathbf{D}_1\mathbf{u})^2+\mathbf{u}(\mathbf{D}_2\mathbf{u}).
\end{aligned}$$

We also have

$$M_{1,h}^k=M_{1,h}[\mathbf{u}^k]:=(\mathbf{u}^k,\mathbf{1})_h, \tag{6.16}$$
$$M_{2,h}^k=M_{2,h}[\mathbf{u}^k]:=(\mathbf{u}^k,(\mathbf{I}_m-\mathbf{D}_2)\mathbf{u}^k)_h, \tag{6.17}$$
$$H_h^k=H_h[\mathbf{u}^k,v_h^k]:=-\frac{1}{2}(\mathbf{u}^k,(\mathbf{u}^k)^2+(\mathbf{D}_1\mathbf{u}^k)^2)_h, \tag{6.18}$$
$$E_h^k=E_h[\mathbf{u}^k,v_h^k]:=-(v_h^k)^2+M_h[\mathbf{u}^k]+H_h[\mathbf{u}_0]. \tag{6.19}$$

Example 6.5 (Non-smooth solution)**.** Consider the problem (2.5) with a non-smooth three-peakon initial condition (see, e.g., [45])

$$u_0(x)=\phi_1(x)+\phi_2(x)+\phi_3(x),$$

where

$$\phi_i(x)=\begin{cases}\dfrac{c_i}{\cosh(L/2)}\cosh(x-x_i), & |x-x_i|\le L/2,\\ \dfrac{c_i}{\cosh(L/2)}\cosh(L-(x-x_i)), & |x-x_i|>L/2,\end{cases} \quad i=1,2,3,$$

and the parameters are selected as $\Omega=[0,30]$, $c_1=2$, $c_2=1$, $c_3=0.8$, $x_1=-5$, $x_2=-3$ and $x_3=-1$.

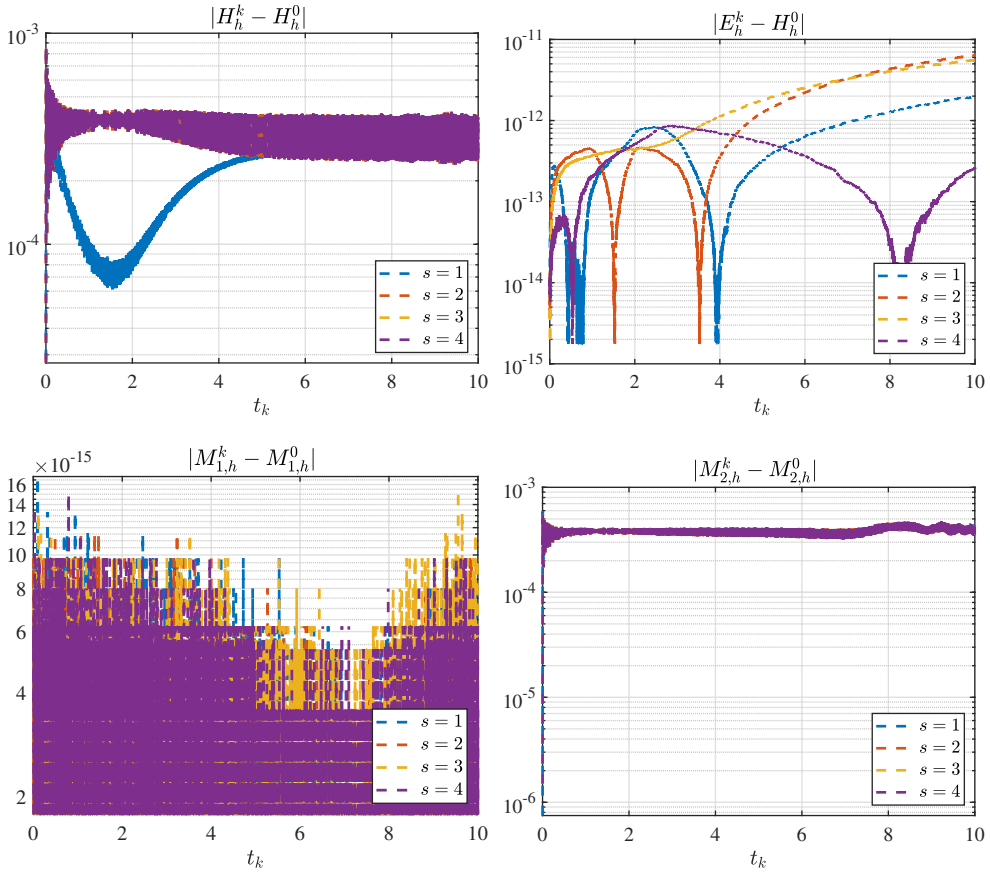

Figure 17: Numerical errors of discrete conservative quantities (6.16)-(6.19) with SAV-RKs in Example 6.5, where $h=30/2048$ and $\tau=1/1000$.

We set $T=10$, $m=2^{11}$, $n=10^4$, and present our numerical results using the SAV-RKs in Figs. 17-19. We observe from Fig. 17 that all SAV-RKs schemes conserve very well the quantities E_h^k and $M_{1,h}^k$. However, H_h^k and $M_{2,h}^k$ are not as well conserved due to the non-smoothness of the exact solution. In Fig. 18, we plot the numerical solution over the time interval [0,10]. We observe that the non-smooth peakons are well resolved without any oscillation, demonstrating superior performance compared to the results in [49]. In Fig. 19, snapshots at various times of the numerical solution obtained using the SAV-RK3 scheme are displayed.

7 Concluding remarks

We construct in this paper a class of nonlinear high-order SAV-RKs methods for general Hamilton systems without assuming a lower bound for the high-order nonlinear part of

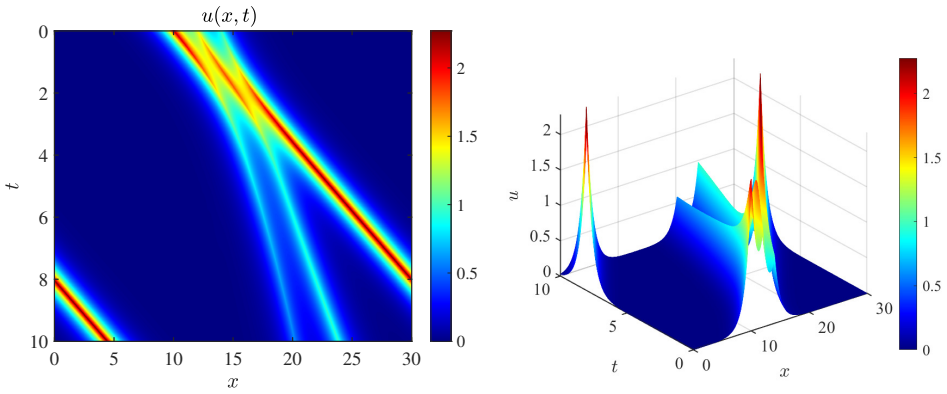

Figure 18: Evolution of numerical solution in Example 6.5 using SAV-RK3 with $h=30/2048$ and $\tau=1/1000$.

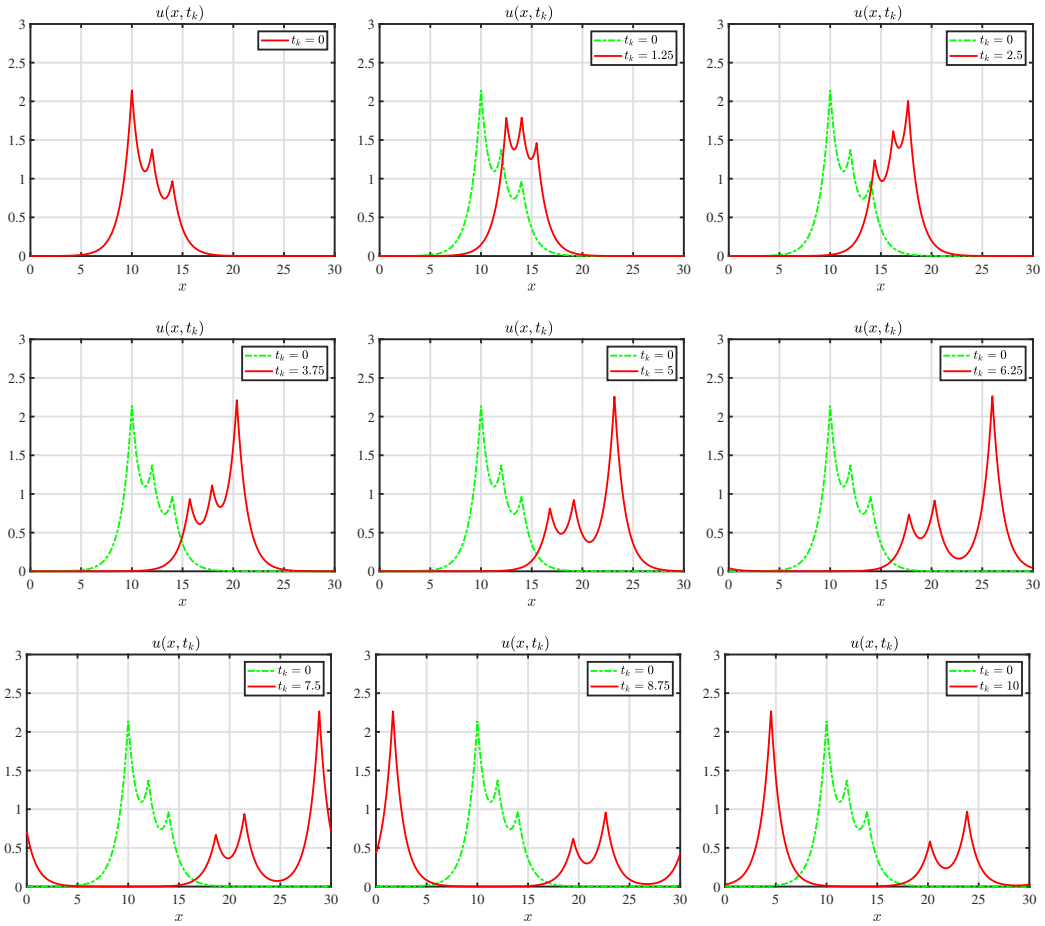

Figure 19: Snapshots of the non-smooth numerical solutions of the CH equation computed by SAV-RK3 with $h=30/2048$ and $\tau=1/1000$ in Example 6.5; Green line denotes snapshot at $t=0$.

the energy. These schemes extend the applicability of the original SAV approach to problems whose high-order part of the energy may not have a lower bound, such as the KdV equation and the DNLSII equation, while still preserve mass and reformulated Hamiltonian energy. In addition, if (1.4) holds, it can also preserve a discrete (1.4) in the absence of spatial discretization error which can be negligible with a spectral discretization.

We developed a fast linearized Newton iteration algorithm for solving the nonlinear system resulting from the SAV-RKs methods, and carried out simulations on a series of typical Hamiltonian systems, including the KdV equation, the DNLS equations and the Camassa–Holm equation, to confirm the effectiveness and robustness of the proposed schemes.

Acknowledgments

The author sincerely thank anonymous referees for their helpful comments and valuable suggestion for the significant improvement of the paper. This work was supported by the Zhejiang Provincial Natural Science Foundation of China under Grant No. LZ23A010007 and the National Natural Science Foundation of China under Grant No. W2431008 and No. 12371409.

Data and codes availability

The data and codes can be found at `https://github.com/zhangqifeng0504/SAV_RKs_Hamilton_system`

Appendix A: The Butcher Tableau

We list below the Butcher Tableau of the s-stage Gaussian-Legendre Runge–Kutta (RKs) method with s=1,2,3,4. For s=1,2,3, the Butcher Tableau is explicitly provided in [15], see (A.1), and for s=4, it can be calculated by symbolic computation based on the collocation method, as presented in [15], see (A.2).

$$\begin{array}{c|c} \frac{1}{2} & \frac{1}{2} \\ \hline & 1 \end{array} \qquad \begin{array}{c|cc} \frac{1}{2}-\frac{\sqrt{3}}{6} & \frac{1}{4} & \frac{1}{4}-\frac{\sqrt{3}}{6} \\ \frac{1}{2}+\frac{\sqrt{3}}{6} & \frac{1}{4}+\frac{\sqrt{3}}{6} & \frac{1}{4} \\ \hline & \frac{1}{2} & \frac{1}{2} \end{array} \qquad \begin{array}{c|ccc} \frac{1}{2}-\frac{\sqrt{15}}{10} & \frac{5}{36} & \frac{2}{9}-\frac{\sqrt{15}}{15} & \frac{5}{36}-\frac{\sqrt{15}}{30} \\ \frac{1}{2} & \frac{5}{36}+\frac{\sqrt{15}}{24} & \frac{2}{9} & \frac{5}{36}-\frac{\sqrt{15}}{24} \\ \frac{1}{2}+\frac{\sqrt{15}}{10} & \frac{5}{36}+\frac{\sqrt{15}}{30} & \frac{2}{9}+\frac{\sqrt{15}}{15} & \frac{5}{36} \\ \hline & \frac{5}{18} & \frac{4}{9} & \frac{5}{18} \end{array} \tag{A.1}$$

$$\begin{array}{c|cccc}
\frac{1}{2}-\frac{\sqrt{\frac{3}{7}+\frac{2\sqrt{30}}{35}}}{2} & \sigma_2 & \frac{1}{8}+\frac{\sqrt{30}}{144}-\sigma_7 & \frac{1}{8}+\frac{\sqrt{30}}{144}-\sigma_6 & \frac{1}{8}-\frac{\sqrt{30}}{144}-\sigma_8 \\
\frac{1}{2}-\frac{\sqrt{\frac{3}{7}-\frac{2\sqrt{30}}{35}}}{2} & \sigma_5+\frac{1}{8}-\frac{\sqrt{30}}{144} & \sigma_3 & \frac{1}{8}+\frac{\sqrt{30}}{144}-\sigma_1 & \frac{1}{8}-\frac{\sqrt{30}}{144}-\sigma_4 \\
\frac{1}{2}+\frac{\sqrt{\frac{3}{7}-\frac{2\sqrt{30}}{35}}}{2} & \sigma_4+\frac{1}{8}-\frac{\sqrt{30}}{144} & \sigma_1+\frac{1}{8}+\frac{\sqrt{30}}{144} & \sigma_3 & \frac{1}{8}-\frac{\sqrt{30}}{144}-\sigma_5 \\
\frac{1}{2}+\frac{\sqrt{\frac{3}{7}+\frac{2\sqrt{30}}{35}}}{2} & \sigma_8+\frac{1}{8}-\frac{\sqrt{30}}{144} & \sigma_6+\frac{1}{8}+\frac{\sqrt{30}}{144} & \sigma_7+\frac{1}{8}+\frac{\sqrt{30}}{144} & \sigma_2 \\
\hline
 & \frac{1}{4}-\frac{\sqrt{30}}{72} & \frac{1}{4}+\frac{\sqrt{30}}{72} & \frac{1}{4}+\frac{\sqrt{30}}{72} & \frac{1}{4}-\frac{\sqrt{30}}{72}
\end{array} \tag{A.2}$$

with

$$\begin{aligned}
&\sigma_1=\frac{\sqrt{15-2\sqrt{30}}\left(8\sqrt{35}+5\sqrt{42}\right)}{840},\quad \sigma_2=\frac{1}{8}-\frac{\sqrt{30}}{144},\quad \sigma_3=\frac{1}{8}+\frac{\sqrt{30}}{144},\\
&\sigma_4=\frac{\sigma_9\left(280\sqrt{3}-161\sqrt{10}+8\sqrt{35}+25\sqrt{42}\right)}{11760},\quad \sigma_5=\frac{\sigma_9\left(161\sqrt{10}-280\sqrt{3}+8\sqrt{35}+25\sqrt{42}\right)}{11760},\\
&\sigma_6=\frac{\sigma_9\left(20\sqrt{3}-13\sqrt{10}+4\sqrt{35}+5\sqrt{42}\right)}{1680},\quad \sigma_7=\frac{\sigma_9\left(13\sqrt{10}-20\sqrt{3}+4\sqrt{35}+5\sqrt{42}\right)}{1680},\\
&\sigma_8=\frac{\sigma_9\left(8\sqrt{35}-5\sqrt{42}\right)}{840},\quad \sigma_9=\sqrt{2\sqrt{30}+15}.
\end{aligned}$$

References

[1] G. Akrivis, B. Li and D. Li, Energy-decaying extrapolated RK–SAV methods for the Allen–Cahn and Cahn–Hilliard equations, SIAM J. Sci. Comput., 41 (6) (2019), A3703–A3727.

[2] H. Bahouri and G. Perelman, Global well-posedness for the derivative nonlinear Schrödinger equation, Invent. Math., 229 (2022), 639–688.

[3] R. Camassa and D. Holm, An integrable shallow water equation with peaked solitons, Phys. Rev. Lett., 71 (11) (1993), 1661.

[4] H. Chen, Y. Lee and C. Liu, Integrability of nonlinear Hamiltonian systems by inverse scattering method, Phys. Scr., 20 (3-4) (1979), 490.

[5] Y. Cheng and C. Shu, A discontinuous Galerkin finite element method for time dependent partial differential equations with higher order derivatives, Math. Comput., 77 (262) (2008), 699–730.

[6] J. Cui, Y. Wang and C. Jiang, Arbitrarily high-order structure-preserving schemes for the Gross–Pitaevskii equation with angular momentum rotation, Comput. Phys. Commun., 261 (2021), 107767.

[7] Y. Cui and D. Mao, Numerical method satisfying the first two conservation laws for the Korteweg–de Vries equation, J. Comput. Phys., 227 (1) (2007), 376–399.

[8] K. Feng and M. Qin, Hamiltonian algorithms for Hamiltonian systems and a comparative numerical study, Comput. Phys. Commun., 65 (1-3) (1991), 173–187.

[9] K. Feng and M. Qin Symplectic Geometric Algorithms for Hamiltonian Systems, Zhejiang Science and Technology Publishing House, Hangzhou; Springer, Heidelberg. 2010.

[10] R. Feynman, A. Hibbs and D. Styer, Quantum Mechanics and Path Integrals, Courier Corporation, 2010.

[11] Y. Fu, D. Hu and Y. Wang, High-order structure-preserving algorithms for the multi-dimensional fractional nonlinear Schrödinger equation based on the SAV approach, Math. Comput. Simul., 185 (2021), 238–255.
[12] Z. Fu, J. Shen and J. Yang, Higher-order energy-decreasing exponential time differencing Runge–Kutta methods for gradient flows, Sci. China Math., 68 (2025), 1727–1746.
[13] Y. Gong, Q. Wang, Y. Wang and J. Cai, A conservative Fourier pseudo-spectral method for the nonlinear Schrödinger equation, J. Comput Phys. 328 (2017), 354–370.
[14] B. Guo, L. Ling and Q. Liu, High-order solutions and generalized Darboux transformations of derivative nonlinear Schrödinger equations, Stud. Appl. Math., 4 (130) (2013), 317–344.
[15] E. Hairer, C. Lubich and G. Wanner, Structure-Preserving Algorithms for Ordinary Differential Equations, Springer-Verlag Berlin, 2006.
[16] J. Hesthaven, S. Gottlieb and D. Gottlieb. Spectral Methods for Time-Dependent Problems, vol. 21. Cambridge University Press, 2007.
[17] H. Holden, K. Karlsen, N. Risebro and T. Tao, Operator splitting for the KdV equation, Math. Comput., 80 (274) (2011), 821–846.
[18] D. Hou, L. Ju and Z. Qiao, Energy-dissipative spectral renormalization exponential integrator method for gradient flow problems, SIAM J. Sci. Comput., 46 (6) (2024), A3477–A3502.
[19] W. Huang and D. Sloan, The pseudospectral method for third-order differential equations, SIAM J. Numer. Anal., 29 (6) (1992), 1626–1647.
[20] A. Jagtap, E. Kharazmi and G. Karniadakis, Conservative physics-informed neural networks on discrete domains for conservation laws: Applications to forward and inverse problems. Comput. Method Appl. M., 365 (15) (2020), 113028.
[21] C. Jiang, Y. Wang and W. Cai, A linearly implicit energy-preserving exponential integrator for the nonlinear Klein-Gordon equation, J. Comput. Phys., 419 (2020), 109690.
[22] C. Jiang, Y. Wang and Y. Gong, Arbitrarily high-order energy-preserving schemes for the Camassa–Holm equation, Appl. Numer. Math., 151 (2020), 85–97.
[23] O. Karakashian and W. McKinney, On optimal high-order in time approximations for the Korteweg–de Vries equation, Math. Comput., 55 (192) (1990), 473–496.
[24] D. Kaup and A. Newell, An exact solution for a derivative nonlinear Schrödinger equation, J. Math. Phys., 19 (4) (1978), 798–801.
[25] T. Kemmochi and S. Sato, Scalar auxiliary variable approach for conservative/dissipative partial differential equations with unbounded energy functionals, BIT Numer. Math., 62 (3) (2022), 903–930.
[26] D. Korteweg and G. de Vries, On the change of form of long waves advancing in a rectangular canal, and on a new type of long stationary waves. Philos. Mag. Serl., 39 (5) (1895), 422–443.
[27] S. Krogstad, Generalized integrating factor methods for stiff PDEs, J. Comput. Phys., 203 (1) (2005), 72–88.
[28] D. Li, X. Li, J. Zhang and Z. Zhang, Stabilized multiple-relaxation implicit-explicit Runge–Kutta methods for nonlinear Gross-Pitaevskii equations, J. Comput. Phys., 538 (2025), 114183.
[29] D. Li, X. Li and Z. Zhang, Implicit–explicit relaxation Runge–Kutta methods: construction, analysis and applications to PDEs, Math. Comput., 92 (339) (2023), 117–146.
[30] M. Li, J. Xiao, W. Liu, Y. Jiang, K. Sun and B. Tian, Breather and double-pole solutions of the derivative nonlinear Schrödinger equation from optical fibers, Phys. Lett. A, 375 (2011), 549–557.
[31] L. Mei and X. Wu, Symplectic exponential Runge–Kutta methods for solving nonlinear

Hamiltonian systems, J. Comput. Phys., 338 (1) (2017), 567–584.
[32] R. Miura, C. Gardner and M. Kruskal, Korteweg-de Vries equation and generalizations. II. Existence of conservation laws and constants of motion, J. Math. Phys., 9 (8) (1968), 1204–1209.
[33] E. Mjølhus, On the modulational instability of hydromagnetic waves parallel to the magnetic field, J. Plasma Phys., 16 (3) (1976), 321–334.
[34] J. Moses, B. Malomed and F. Wise, Self-steepening of ultrashort optical pulses without self-phase-modulation, Phys. Rev. A, 76 (2) (2007), 021802.
[35] J. Pu and Y. Chen, Lax pairs informed neural networks solving integrable systems. J. Comput. Phys., 510 (2024), 113090.
[36] J. Shen and T. Tang, Spectral and High-Order Methods with Applications, Science Press Beijing, 2006.
[37] J. Shen and J. Xu, Convergence and error analysis for the scalar auxiliary variable (SAV) schemes to gradient flows, SIAM J. Numer. Anal., 56 (5) (2018), 2895–2912.
[38] J. Shen, J. Xu and J. Yang, The scalar auxiliary variable (SAV) approach for gradient flows, J. Comput. Phys., 353 (2018), 407–416.
[39] T. Tang, X. Wu and J. Yang, Arbitrarily high order and fully discrete extrapolated RK-SAV/DG schemes for phase-field gradient flows, J. Sci. Comput., 93 (2022), Article 38.
[40] L. Trefethen, Spectral Methods in MATLAB, vol. 10. SIAM, 2000.
[41] N. Tzoar and M. Jain, Self-phase modulation in long-geometry optical waveguides, Phys. Rev. A, 23 (3) (1981), 1266.
[42] J. Verwer, Conservative and nonconservative schemes for the solution of the nonlinear Schrödinger equation, IMA J. Numer. Anal., 6 (1986), 25–42.
[43] D. Wang, A. Xiao and X. Li, Parametric symplectic partitioned Runge–Kutta methods with energy-preserving properties for Hamiltonian systems, Comput. Phys. Commun., 184 (2) (2013), 303–310.
[44] K. Wu, T. Qin and D. Xiu, Structure-preserving method for reconstructing unknown Hamiltonian systems from trajectory data. SIAM J. Sci. Comput., 42(6) (2020), A3704–A3729.
[45] Y. Xu and C. Shu, A local discontinuous Galerkin method for the Camassa–Holm equation, SIAM J. Numer. Anal., 46 (4) (2008), 1998–2021.
[46] Y. Xu and C. Shu, Local discontinuous Galerkin methods for nonlinear Schrödinger equations, J. Comput. Phys., 205 (1) (2005), 72–97.
[47] K. Yang, Arbitrarily high-order conservative schemes for the generalized Korteweg-de Vries equation, SIAM J. Sci. Comput., 44 (4) (2022), A2709–A2733.
[48] K. Yang, High order conservative schemes for the generalized Benjamin-Ono equation on the unbounded domain. J. Sci. Comput., 96 (2023), Article 35.
[49] T. Yan, J. Zhang and Q. Zhang, Fully conservative difference schemes for the rotation-two-component Camassa–Holm system with smooth/nonsmooth initial data, Wave Motion, 129 (2024), 103333.
[50] X. Yang and D. Han, Linearly first-and second-order, unconditionally energy stable schemes for the phase field crystal model, J. Comput. Phys., 330 (2017), 1116–1134.
[51] H. Zhang, X. Qian, J. Yan and S. Song, Highly efficient invariant-conserving explicit Runge–Kutta schemes for nonlinear Hamiltonian differential equations, J. Comput. Phys., 481 (1) (2020), 109598.
[52] Y. Zhang, L. Guo, J. He and Z. Zhou, Darboux transformation of the second-type derivative nonlinear Schrödinger equation, Lett. Math. Phys., 105 (2015), 853–891.